Contrib Mineral Petrol (2005) 148: 542–565
DOI 10.1007/s00410-004-0619-6

ORIGINAL PAPER

Timothy L. Grove · Michael B. Baker · Richard C. Price
Stephen W. Parman · Linda T. Elkins-Tanton
Nilanjan Chatterjee · Othmar Müntener

Magnesian andesite and dacite lavas from Mt. Shasta, northern California: products of fractional crystallization of H_2O-rich mantle melts

Received: 13 January 2004 / Accepted: 1 September 2004 / Published online: 10 November 2004

Abstract Mt. Shasta andesite and dacite lavas contain high MgO (3.5–5 wt.%), very low FeO*/MgO (1–1.5) and 60–66 wt.% SiO_2. The range of major and trace element compositions of the Shasta lavas can be explained through fractional crystallization (~50–60 wt.%) with subsequent magma mixing of a parent magma that had the major element composition of an H_2O-rich primitive magnesian andesite (PMA). Isotopic and trace element characteristics of the Mt. Shasta stratocone lavas are highly variable and span the same range of compositions that is found in the parental basaltic andesite and PMA lavas. This variability is inherited from compositional variations in the input contributed from melting of mantle wedge peridotite that was fluxed by a slab-derived, fluid-rich component. Evidence preserved in phenocryst assemblages indicates mixing of magmas that experienced variable amounts of fractional crystallization over a range of crustal depths from ~25 to ~4 km beneath Mt. Shasta. Major and trace element evidence is also consistent with magma mixing. Pre-eruptive crystallization extended from shallow crustal levels under degassed conditions (~4 wt.% H_2O) to lower crustal depths with magmatic H_2O contents of ~10–15 wt.%. Oxygen fugacity varied over 2 log units from one above to one below the Nickel-Nickel Oxide buffer. The input of buoyant H_2O-rich magmas containing 10–15 wt.% H_2O may have triggered magma mixing and facilitated eruption. Alternatively, vesiculation of oversaturated H_2O-rich melts could also play an important role in mixing and eruption.

Editorial Responsibility: J. Hoefs

T. L. Grove (✉) · S. W. Parman · N. Chatterjee
Department of Earth, Atmospheric and Planetary Sciences,
Massachusetts Institute of Technology,
Cambridge, MA, 02139, USA
E-mail: tlgrove@mit.edu
Tel.: +1-617-2532878
Fax: +1-617-2537102

M. B. Baker
Division of Geological and Planetary Sciences,
California Institute of Technology,
Pasadena, CA 91125, USA

R. C. Price
School of Science and Technology,
University of Waikato, Private Bag 3105,
Hamilton, New Zealand

L. T. Elkins-Tanton
Department of Geological Sciences,
Brown University, Providence,
02912, Rhode Island

O. Müntener
Institut de Géologie, Université de Neuchâtel,
2007 Neuchatel, Switzerland

Introduction

Mt. Shasta is the largest of the andesitic stratocone volcanoes in the Cascade Range and it has erupted over 500 km^3 of andesite and dacite lava over the past ~200,000 years. In a previous paper (Grove et al. 2002) we have provided a model for magmatic processes that led to the formation of primitive lavas in the Mt. Shasta region. The purpose of this work is to explore the relationship between these rare primitive magmas and the more voluminous eruptive products of the Mt. Shasta stratocone. The stratocone lavas define an end member (Fig. 1) among the global variations spanned by subduction-related andesites (Ewart 1979; Gill 1981). This end member is characterized by an extremely low FeO*/MgO at high SiO_2 (Fig. 1a). Lavas with major and trace element characteristics similar to some of those found at Mt. Shasta have been termed adakites; the high-Mg andesites of the western Aleutians (Kay 1978; Yogodzinski et al. 1995, Fig. 1b). The distinctive major and trace element signatures of andesite lavas of the Setouchi belt of SW Japan (sanukitoids, Tatsumi and Ishizaka 1982, Fig. 1b) are also shared by some Mt. Shasta lavas. Arc-related lavas

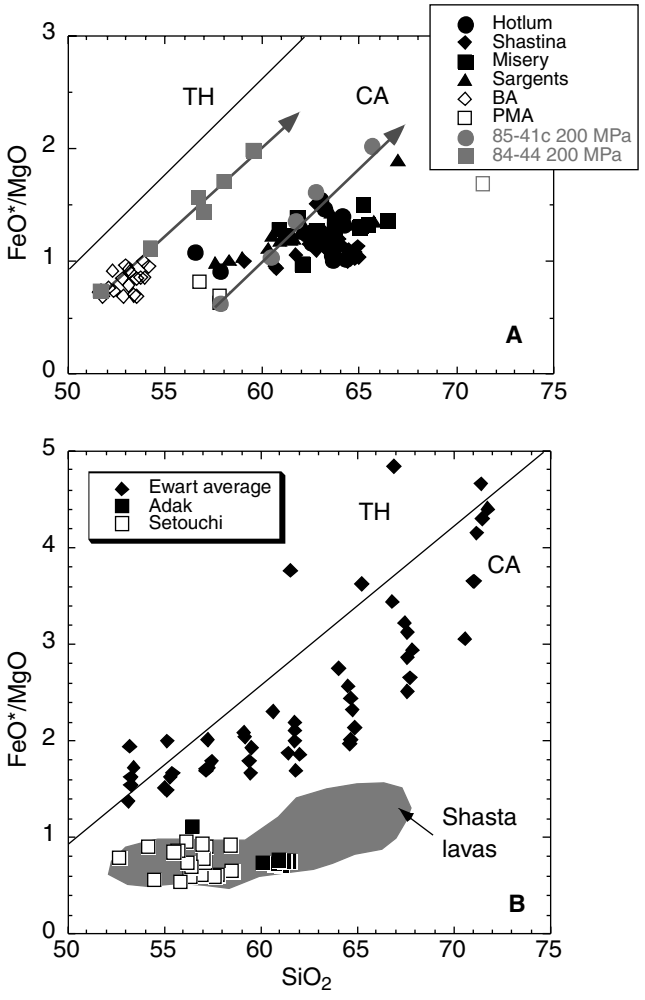

Fig. 1 **a** Compositional characteristics of andesites, dacites and associated primitive lavas of the Mt. Shasta region. FeO*/MgO vs. SiO_2 diagram shows the calc-alkaline dividing line from Irvine and Baragar (1971). Also shown are the compositions of liquids produced from H_2O-saturated crystallization experiments on primitive magnesian andesite 85-41c and basaltic andesite 85-44 at 200 MPa and the NNO buffer. **b** Mt. Shasta lavas compared with average global arc lava suites from Ewart (1979, 1982) (solid diamonds) and other high-Mg andesites (adakites, Kay 1978; Yogodzinski et al. 1995) and lavas from the Setouchi belt in the SW Japan arc (Tatsumi and Ishizaka 1982)

like the Aleutian adakites, Setouchi andesites and Shasta andesites are all associated with the subduction of young oceanic crust.

In other settings similar rocks have been interpreted in terms of subducted slab melting, with or without subsequent reaction with mantle wedge peridotite (see Grove et al. 2002). The andesite and dacite lavas of Mt. Shasta preserve evidence in their mineral textural and compositional relations of the magmatic processes that led to their formation. In the following discussion, we describe the petrologic and geochemical diversity of these rocks and use this evidence along with constraints from experimental petrology to develop a model for the origin of these high-Mg andesites.

Geologic setting and sampling

Mt. Shasta is situated near the southern end of the Cascade chain and is flanked to the south and west by pre-Tertiary rocks of the Klamath Mountain province and to the northeast and east by Tertiary and Quaternary volcanics of the High Cascades. Medicine Lake volcano, a large shield volcano consisting of basalt to rhyolite lavas lies ~60 km to the east and the Lassen Volcanic Field is ~130 km to the southeast. Tertiary sandstones, shales, and andesitic volcanics, Mesozoic granitic rocks, ultramafic rocks of the Trinity ophiolite, and Mesozoic and Paleozoic metasedimentary rocks are present in the Shasta region and have been inferred to be present beneath the volcano (Griscom 1980; Blakely et al. 1985; Fuis et al. 1987). Mt. Shasta is situated at the western end of a gravity low that has been named the Shasta gravity lineament (Blakeley et al. 1997). Mt. Shasta is also situated at the western end of a region of anomalously low P-wave velocity that extends throughout the upper 30 km of the crust (Benz et al. 1992). This region could represent elevated crustal temperatures or lithologic variations.

Early work on Mt. Shasta is summarized by Williams (1932a, b, 1934, 1949); MacDonald (1966). Christiansen et al. (1977; unpublished mapping) delineates four major episodes of andesite cone building at Mt. Shasta. Miller (1978, 1980) discusses the Holocene eruptive history of Shastina and Black Butte. Geochemistry and petrology of Mt. Shasta lavas are presented by Smith and Carmichael (1968), Condie and Swenson (1973), Anderson (1974a), Newman et al. (1986), Baker (1988) and Volpe (1992). Most of the stratocone lavas could be (and have been) classified as two-pyroxene andesites, but this nomenclature belies the rich petrologic complexity present in the phenocryst assemblages of these rocks. A more appropriate classification would be multi-pyroxene andesites, and the significance of this mineralogical diversity is one focus of this contribution. Dacites (up to 66 wt.% SiO_2) also occur as lava flows on the stratocone and additionally as flank domes and plugs. Rare rhyodacite is also present. Small volumes of primitive magnesian andesite (PMA), basaltic andesite (BA) and high-alumina olivine tholeiite (HAOT) are present as cinder cones and lava flows on the flanks of the stratocone (Baker et al. 1994; Bacon et al. 1997; Grove et al. 2002, 2003).

In order of decreasing age the major cone-building episodes delineated by Christiansen et al. (1977) are: Sargents Ridge (~250,000 to ~130,000 years before present (ybp)), Misery Hill (80,000—10,000 ybp), Shastina (~10,000–9,400 ybp) and Hotlum (~6,000–2,000 ybp, with eruptive activity possibly occurring as recently as 1786 A.D.). The earliest formed eruptive center, the Sargents Ridge cone, now constitutes the south flank of the volcano. Andesite and dacite lava flows and pyroclastic flows were erupted from a vent that is now deeply eroded and glaciated. Domes were

also erupted around the flanks of the volcano during this stage of activity. The Misery Hill Cone is 0.5 km south of the summit of Shasta (~13,800') and is the next youngest eruptive center of the Mt. Shasta edifice. Lavas and pyroclastic flows erupted from this vent which contains a dacite summit dome. A pumice flow (informally known as the Red Banks) represents the last eruptive event of the Misery Hill stage. The third major episode of volcanism occurred at Shastina (12,330'), a vent that lies 2.5 km to the west of the summit of Mt. Shasta (Fig. 2). Late dacite domes were emplaced within Shastina's summit crater, and andesite and dacite lavas and pyroclastic flows erupted from the Shastina vent and flowed down the northwestern, western and southwestern flanks. The Lava Park Flow (7.5 km NW of Shastina summit at 6,000') is an andesitic flank eruption of the Shastina stage, and Black Butte (12.3 km W of Shastina summit at 6358') is a plug that erupted hornblende dacite at ~9400 ybp (Miller 1978, 1980). The last and youngest eruptive phase of the stratocone, the Hotlum Cone forms the current summit of Mt. Shasta (14,162'). Dacite domes and flows are present near the summit. Andesite and dacite lavas and pyroclastic flows erupted from summit vents and flowed down the north and northeastern flanks of the cone (Fig. 2). Hot springs are currently active near the summit of Mt. Shasta and the last eruption of Hotlum may have occurred as recently as 1786 (Harris 2003).

Andesite lavas were sampled from the upper and lower extremes of the Holocene eruptive stages (Shastina and Hotlum) as were summit dacite domes. For these younger stages, samples were also collected along the entire length of several large flows from the summit (4,300 m) down to 1,200 m to check for compositional zoning. None was found and each lava flow has a nearly constant major element composition and possesses unique trace element characteristics. The older eruptive phases of the volcano (Sargents Ridge and Misery) have been modified by glaciation(s). Samples of the Misery stage (Fig. 2) were collected from high on the stratocone and from flank dacite vents. Samples of the Sargents Ridge stage were taken from the glacially eroded summit

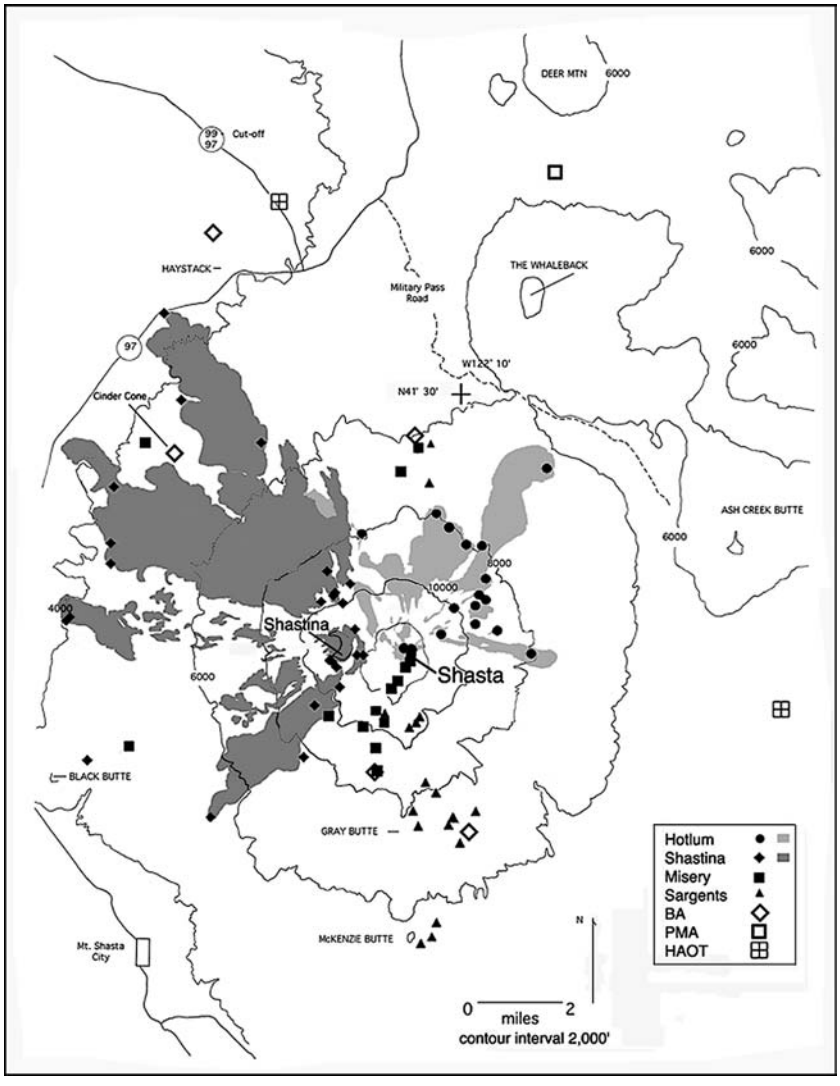

Fig. 2 Map of the Mt. Shasta region showing the approximate locations of samples described in this paper. See Table 1 for locations. The outlines of lava flows from the Hotlum (*light gray*) and Shastina (*darker gray*) eruptive phases are also shown. *Symbols* indicate eruptive stage of samples. *Solid circles* Hotlum, *solid diamonds* Shastina, *solid squares* Misery, *solid triangles* Sargents. The locations of primitive lavas described in Grove et al. (2002, 2003) are: *open square* PMA, *open diamonds* BA and *square with cross* HAOT

lavas on the southern side of Mt. Shasta and from surrounding flank vents to the south and north of the stratocone. An older flank eruption of the Sargents Ridge phase, McKenzie Butte produced rhyodacite lavas that are also discussed in this paper.

Analytical methods

Major and trace element whole-rock compositions on the 82-, 83-, and 85-series samples were obtained by wavelength dispersive X-ray fluorescence spectroscopy (XRF) at La Trobe University, Bundoora, Australia, following the techniques of Norrish and Hutton (1969) and Norrish and Chappel (1977). FeO was determined by wet chemistry. See Baker et al. (1994) for analytical details. Based on four pairs of replicate analyses, percent error for major elements is generally less than 0.5%; exceptions are TiO_2, MgO and K_2O, 1–2%, and P_2O_5, ~6%. Trace element precision is generally better than 5%. For samples with the prefixes 95-, 96-, 97- and 99- major-element compositions were determined by wavelength dispersive XRF at the US Geological Survey (USGS) laboratory in Lakewood, CO. Trace element contents of these lavas were analyzed by energy dispersive XRF at the USGS in Menlo Park, CA, USA. Analytical uncertainties reported by Bacon and Druitt (1988) provide an estimate of the errors associated with the USGS analyses. All major-element analyses are reported in Table 1 and XRF trace-element analyses are reported in Table 2.

For a subset of the samples discussed in this paper selected trace and rare-earth elements were also measured by inductively-coupled plasma mass spectrometry (ICP-MS). These analytical data are reported in Grove et al. (2002). The isotopic compositions of Pb, Nd and Sr were determined at MIT for a subset of the andesites and dacite described in this paper. These analytical data can also be found in Grove et al. (2002).

Compositions of minerals in the Shasta lavas were obtained with the MIT three-spectrometer MAC-5 microprobe and five-spectrometer JEOL 733 Superprobe using two on-line data reduction procedures. All analyses were performed using a 15 kV accelerating voltage and a 10 nA beam current. For samples with the 82-, 83-, and 85- designation the matrix correction procedures of Bence and Albee (1968) were used with modifications of Albee and Ray (1970). For samples in the 95-, 96-, 97- and 99- series newer automation software was employed that utilized the CITZAF correction package of Armstrong (1995). The atomic number correction of Duncumb and Reed, Heinrich's tabulation of absorption coefficients, and the fluorescence correction of Reed were used to obtain quantitative analyses. A comparison of the two techniques on working standards of plagioclase, orthopyroxene and clinopyroxene showed no appreciable difference between the results obtained by the two methods. Analyses of a representative subset of minerals are presented in Table 3. See Gaetani and Grove (1998) for a discussion of analytical precision.

Major and trace element compositions

Major elements and pre-eruptive H_2O contents

Mt. Shasta lavas are classified as andesites if they have <64 wt.% SiO_2, dacites if SiO_2 falls between 64 and 68 wt.% and rhyodacites if SiO_2 is >68 wt.%. Many Shasta andesites and dacites have extremely low FeO*/MgO and therefore have high Mg#s (60–65) (where Mg# = 100*Mg/(Mg + Fe*), atomic, where Fe* equals all Fe as Fe^{2+}); such values are unusually high for andesites with such high SiO_2 contents (Fig. 1). The most primitive Shasta andesites have MgO contents of 3.5 to >5 wt.% MgO with SiO_2 contents that range from ~59–62 wt.%. Some samples that contain >5 wt.% MgO (99-12A and 12B) are mafic inclusions or mafic end members of a mixed lava flow (85-55 and 85-56, informally referred to as the Panther Creek flow). Alumina contents span a range of 16–18 wt.% (Fig. 3a) and there is no systematic correlation of Al_2O_3 abundance with modal% plagioclase in the sampled population (Baker 1988). Abundances of CaO (Fig. 3c), FeO* (total Fe as FeO) and TiO_2 decrease as MgO decreases (e.g., Fig. 3f) while K_2O and Na_2O abundances increase with decreasing MgO (Fig. 3d, e). Also plotted in Fig. 3 are the compositions of primitive Shasta-region lavas (BA, PMA), along with experimentally produced liquid lines of descent on BA and PMA compositions at 200 MPa, H_2O saturated at the NNO (nickel—nickel oxide) buffer and 0.1 MPa anhydrous at the QFM (quartz—fayalite—magnetite) buffer (see Baker et al. 1994; Grove et al. 2003).

Anderson (1974a, b, 1976, 1979) inferred the H_2O contents of andesitic magmas from the Shasta region by measuring the major element composition of trapped melt inclusions in pyroxene and plagioclase and assuming that the summation deficit reflected the H_2O content of melt. Anderson's (1979, see his Fig. 8) highest estimated water contents (~6–8 wt.% H_2O) were from melt inclusions in stratocone lavas and in a Shastina-age dacite from the Shastina summit domes, which were estimated to contain ~10–13 wt.% H_2O (Anderson 1979, sample S76). The same melt inclusion for which Anderson (1979) obtained an H_2O content of 13 wt.%, using the summation deficit method, was reanalyzed by Grove et al. (2003) and an estimate of 10.8 wt.% H_2O was obtained from a quantitative measurement of oxygen abundance.

Trace element compositional variations

The variations in selected trace element abundances are shown on MgO variation diagrams in Fig. 4 for the Shasta andesite, dacite and rhyodacite lavas. There is a

Table 1 Major element compositions of andesite and dacite lavas from the Mt. Shasta region

	SiO_2	TiO_2	Al_2O_3	Fe_2O_3	FeO	MnO	MgO	CaO	Na_2O	K_2O	P_2O_5	LOI	Sum	Lab	N41	W122
Hotlum																
82-91a	63.14	0.57	16.88	1.54	2.43	0.07	3.59	5.89	4.11	1.18	0.17	0.30	99.57	1	28.34	7.88
82-91b	63.32	0.57	16.73	1.51	2.39	0.07	3.71	6.02	4.09	1.11	0.17	0.26	99.69	1	28.34	7.88
82-96	62.96	0.58	17.01	1.47	2.71	0.08	3.44	5.93	4.19	1.20	0.16	0.25	99.73	1	27.33	10.77
82-97	63.38	0.59	16.62	3.82	0.83	0.07	3.03	5.19	4.00	1.56	0.14	0.47	99.23	1	24.54	11.67
83-44	62.26	0.61	16.93	1.92	2.64	0.08	3.49	5.99	4.60	1.23	0.16	0.55	99.91	1	24.53	8.33
83-45	62.98	0.52	17.51	2.93	1.24	0.08	2.64	5.52	4.93	1.27	0.16	0.98	99.78	1	25.00	9.22
83-46	62.88	0.63	17.25	1.56	2.98	0.09	2.84	5.61	4.77	1.26	0.16	0.44	100.03	1	25.17	9.86
83-54	63.80	0.59	16.14	2.68	1.69	0.08	3.11	5.31	4.59	1.57	0.13	0.77	99.69	1	24.63	11.53
83-55	62.44	0.63	16.36	2.11	2.58	0.08	3.52	5.89	4.32	1.41	0.14	0.61	99.48	1	24.66	11.6
97-4	62.21	0.61	17.03	4.86		0.08	3.45	5.95	4.16	1.26	0.18	0.01	99.78	2	25.63	9.6
97-5	61.85	0.64	16.94	4.58		0.07	3.46	6.02	4.14	1.24	0.23	0.46	99.18	2	25.44	10.41
97-6	61.51	0.65	16.81	4.65		0.08	3.57	6.06	4.10	1.23	0.23	0.60	98.87	2	26.08	9.55
99-12A	56.90	0.36	17.10	5.98		0.11	5.90	8.82	3.03	0.74	0.13	0.40	99.07	2	25.55	9.81
99-12B	55.70	0.54	16.80	7.29		0.14	6.08	9.23	2.88	0.48	0.13	0.19	99.27	2	25.55	9.81
99-13	61.50	0.60	17.00	4.88		0.08	3.47	5.97	3.95	1.24	0.23	0.20	98.92	2	24.92	10.75
99-14	61.70	0.60	17.00	4.77		0.08	3.45	5.92	4.00	1.23	0.23	0.24	98.98	2	24.92	10.76
99-15	61.30	0.64	16.80	4.56		0.08	3.42	5.88	3.98	1.25	0.27	0.71	98.18	2	25.79	10.17
99-16	61.50	0.65	16.70	4.62		0.08	3.53	6.02	3.98	1.24	0.27	0.56	98.59	2	25.72	9.75
99-17	62.40	0.57	17.00	4.31		0.07	3.21	5.86	4.06	1.20	0.22	0.43	98.90	2	27.05	10.35
99-18	61.40	0.65	16.80	4.62		0.08	3.53	6.07	3.98	1.23	0.27	0.45	98.63	2	26.77	10.06
99-19	62.80	0.58	16.20	3.98		0.06	3.50	5.87	3.87	1.00	0.21	0.74	98.07	2	26.75	9.65
Shastina																
82-82	62.49	0.56	16.31		5.21	0.07	3.45	5.94	4.15	1.12	0.19	0.36	99.49	1	29.76	17.79
83-50	63.38	0.60	16.13	1.78	2.41	0.07	3.70	6.09	4.58	1.14	0.20	0.34	100.08	1	26.2	13.2
83-51	62.43	0.61	16.29	1.58	2.78	0.08	3.82	6.11	4.59	1.12	0.19	0.87	99.60	1	25.78	13.63
83-52	63.35	0.61	16.24	1.51	2.64	0.08	3.65	6.05	4.60	1.14	0.19	0.35	100.06	1	25.37	13.87
83-53	63.03	0.61	16.28	1.42	2.70	0.07	3.60	6.00	4.58	1.16	0.19	0.84	99.64	1	25.73	13.65
83-57	64.47	0.49	16.33	1.90	1.72	0.07	3.34	5.97	4.25	0.99	0.14	0.30	99.67	1	24.51	13.04
83-58	63.89	0.56	16.54	1.72	2.10	0.07	3.22	6.06	4.27	1.11	0.16	0.52	99.70	1	23.85	13.51
85-3	61.20	0.68	16.22	0.67	3.81	0.09	4.18	6.56	4.06	1.03	0.23	1.44	98.73	1	27.96	19.59
95-12c	62.80	0.59	16.50	4.42		0.07	3.46	5.88	3.95	1.17	0.25	0.74	99.09	2	25.57	13.4
95-13	64.20	0.49	16.80	3.83		0.06	3.32	5.98	4.03	1.00	0.16	0.18	99.87	2	26.22	13.85
96-1	63.20	0.57	16.83	4.12		0.07	3.28	6.00	4.00	1.16	0.19	0.57	99.40	2	21.28	16.8
96-5	63.75	0.48	16.73	3.82		0.06	3.43	6.01	4.03	0.98	0.13	0.15	99.43	2	25.2	13.06
96-7	63.29	0.54	16.83	4.09		0.08	3.07	6.06	4.05	1.17	0.16		99.34	2	23.45	14.17
96-10a	62.96	0.56	16.85	4.05		0.07	3.24	6.00	4.04	1.12	0.19	0.87	99.08	2	25.2	13.06
96-11b	64.25	0.51	16.82	3.76		0.07	2.99	5.89	3.86	1.07	0.15		99.37	2	24.39	13.76
96-12	64.06	0.49	16.86	3.79		0.06	3.25	5.94	4.04	1.01	0.14	0.16	99.64	2	24.36	13.69
96-13	64.22	0.49	16.81	3.82		0.06	3.30	5.93	4.07	0.99	0.14	0.12	99.83	2	24.24	13.58
97-3	59.27	0.79	15.90	4.85		0.08	4.64	6.70	3.69	1.79	0.41	1.39	98.11	2	25.3	20.77
97-7	63.02	0.59	16.55	4.25		0.07	3.51	6.02	4.12	1.14	0.21	0.08	99.48	2	24.49	12.85
99-4	59.10	0.79	15.80	4.94		0.08	4.68	6.67	3.69	1.79	0.46	1.19	98.00	2	25.21	20.84
99-5	61.30	0.64	17.00	4.54		0.07	3.54	6.26	4.03	1.03	0.25	0.79	98.66	2	26.8	19.69
99-6	57.80	0.86	16.20	5.79		0.09	5.23	7.62	3.58	1.00	0.33	0.40	98.50	2	26.4	19.69
99-7	62.60	0.55	16.00	3.99		0.07	3.25	6.15	3.66	1.07	0.23	1.70	97.57	2	28.89	15.62
99-10	64.40	0.43	17.60	3.58		0.06	2.07	5.23	4.32	1.18	0.19	0.01	99.06	2	22.31	20.31
99-11	62.10	0.57	16.60	4.20		0.07	3.31	5.99	3.80	1.15	0.24	1.06	98.03	2	31.56	18.24
Misery																
82-93	62.15	0.64	17.23	0.75	3.54	0.08	3.10	5.51	3.98	1.41	0.18	1.06	98.57	1	28.29	11.84
82-94d	60.83	0.71	17.71	4.14	0.65	0.08	3.14	6.43	3.88	1.03	0.22	1.22	98.82	1	28.76	11.37
82-98	63.25	0.60	16.65	1.37	2.87	0.08	3.20	5.50	4.05	1.56	0.18	0.84	99.31	1	24.36	11.59
82-99	61.56	0.60	16.74	1.55	2.89	0.08	3.37	5.94	4.05	1.25	0.15	1.70	98.18	1	24.26	11.70
82-100	63.95	0.50	16.99	1.95	1.65	0.07	2.27	4.98	4.55	1.22	0.15	1.74	98.28	1	23.95	11.93
82-101	63.91	0.47	16.87	2.18	1.30	0.06	2.48	5.12	4.59	1.31	0.13	1.13	98.42	1	23.80	12.10
82-103	60.47	0.63	17.45	1.33	3.61	0.09	3.75	6.60	4.09	1.26	0.13	1.21	99.41	1	23.11	12.30
82-104	64.92	0.48	17.23	1.27	2.19	0.06	2.58	5.22	4.59	1.31	0.13	0.37	99.98	1	23.01	12.84
82-105	60.86	0.61	17.70	1.92	2.73	0.08	3.65	6.36	4.30	1.19	0.15	0.35	99.55	1	22.57	12.52
83-49	63.42	0.60	16.19	1.63	2.54	0.07	3.55	5.97	4.58	1.17	0.19	0.50	99.91	1	27.03	13.03
83-56	65.62	0.44	16.64	1.76	1.36	0.05	2.16	4.86	4.60	1.36	0.12	1.17	98.97	1	23.34	12.52
83-59	65.28	0.49	16.70	1.48	2.03	0.06	2.55	5.23	4.66	1.30	0.12	0.31	99.90	1	23.24	13.81
85-2a	62.50	0.63	16.99	0.88	3.16	0.07	3.33	6.22	4.01	1.16	0.17	0.75	99.12	1	28.89	18.76
85-2b	62.67	0.64	16.75	0.18	3.83	0.07	3.36	6.28	4.07	1.15	0.18	0.43	99.18	1	28.89	18.76
85-48b	61.84	0.71	16.47	1.17	2.97	0.08	4.11	6.81	4.12	0.86	0.18	0.84	99.32	1	22.11	12.48
99-9	63.70	0.53	16.50	3.91		0.06	2.85	4.77	3.96	1.78	0.19	0.95	98.25	2	22.61	19.43

Table 1 (Contd.)

	SiO_2	TiO_2	Al_2O_3	Fe_2O_3	FeO	MnO	MgO	CaO	Na_2O	K_2O	P_2O_5	LOI	Sum	Lab	N41	W122
Sargents																
82-83	61.59	0.59	17.70	1.30	3.44	0.09	3.31	5.95	4.23	1.48	0.16	0.47	99.84	1	21.25	11.51
82-84a	61.37	0.58	17.78	1.94	2.80	0.07	3.46	6.21	4.72	1.16	0.49	0.67	100.58	1	20.98	11.38
82-85	61.00	0.66	16.86	0.76	3.86	0.08	3.80	5.83	4.37	1.81	0.30	0.68	99.33	1	21.67	10.89
82-86	61.96	0.66	17.36	1.36	3.38	0.09	3.52	6.00	4.03	1.33	0.17	0.33	99.86	1	21.86	11.15
82-87	61.19	0.59	17.84	1.60	2.68	0.07	3.28	6.27	4.23	1.12	0.15	0.60	99.02	1	22.99	11.61
82-88b	62.98	0.58	16.74	1.60	2.55	0.07	2.79	5.12	4.65	1.93	0.28	0.99	99.29	1	23.21	11.28
82-89	65.26	0.51	15.86	3.17	0.88	0.07	2.76	4.80	3.94	2.11	0.17	0.66	99.53	1	23.07	11.42
82-92a	66.38	0.45	16.37		3.59	0.06	1.89	4.18	4.10	1.94	0.13	1.30	99.09	1	28.06	11.10
82-95	63.95	0.61	16.05	1.79	2.59	0.08	3.17	5.05	3.88	2.21	0.18	0.34	99.56	1	28.84	11.06
82-102	60.61	0.65	16.97	1.49	3.57	0.09	4.15	6.79	3.91	1.23	0.16	0.36	99.62	1	23.26	12.25
85-55	57.74	0.75	16.08	1.23	4.23	0.11	5.28	8.65	3.77	1.30	0.29	1.03	99.43	1	20.61	10.23
85-56	56.93	0.76	16.29	1.72	3.96	0.11	5.55	8.21	3.56	1.16	0.30	1.73	98.55	1	21.01	10.51
85-57b	58.24	0.71	16.21	1.61	3.68	0.11	4.96	7.83	3.71	1.15	0.27	0.94	98.48	1	21.12	10.41
85-58	59.85	0.71	16.60	2.05	3.22	0.10	4.13	6.68	3.67	1.50	0.24	0.78	98.75	1	21.12	10.43
85-59	59.88	0.72	16.26	2.36	2.68	0.09	4.29	6.14	4.55	1.82	0.34	0.75	99.13	1	21.29	9.82
75-22	68.80	0.32	16.10	1.05	1.67	0.06	0.53	2.31	4.70	2.64	0.10	1.76	98.28	1	18.55	11.28
85-42	63.48	0.38	18.72	1.54	1.69	0.08	0.58	2.54	6.18	1.72	0.11	3.09	97.02	1	18.99	10.87
85-43	69.89	0.29	14.64	1.63	1.03	0.07	0.47	1.79	6.00	2.74	0.09	1.24	98.64	1	18.65	11.01

Latitude (N41) and longitude (W122) values for each sample are given in minutes from 41°N and 122°W
Lab number indicates analysis location. *1* analysis performed at LaTrobe University. *2* analysis performed at U.S. Geological Survey
An empty space in either the FeO or Fe_2O_3 column indicates that FeO was not determined or that analysis reported all Fe as FeO or Fe_2O_3
All oxide concentrations are in wt.%

wide range of variation in the abundance of the large ion lithophile elements (e.g., Sr and Ba, Fig. 4a, c) in lavas produced during each eruptive phase. Among other incompatible elements, Rb abundance varies by almost a factor of 4 within the andesite-dacite compositional range, while Zr varies by a factor of 2.7. The abundance of Ce also varies by a factor of 2.7 within the stratocone andesite lavas. A characteristic of each eruptive episode seems to be large variations in trace element abundances, and where multiple samples of single flows are available we find that the trace elements are constant in each flow and variable between flows. Also shown in Fig. 4 are trace element compositions for the primitive Shasta region lavas. The PMAs and BAs exhibit much less trace element variation than the andesites and dacites, but they still vary by a factor of 2 in Sr, Ba, Ce, Zr and Rb (Fig. 4a–e). PMA and BA lavas are strongly enriched in the compatible elements Ni and Cr (Fig. 4f, g) relative to the stratocone lavas. We will argue that the observed incompatible trace element variations in the sampled BA and PMA lavas are not representative of the entire input of these primitive magmas into the volcanic system. Grove et al. (2002) attribute this elemental variability to a heterogeneous input of a fluid-rich, slab-derived component that leads to flux-melting of the mantle wedge.

Isotopic compositional variations

The variations in $^{87}Sr/^{86}Sr$ and $^{143}Nd/^{144}Nd$ (ε_{Nd}) isotopic ratios are plotted in Fig. 5 for Shasta primitive lavas and stratocone andesite and dacite lavas (see Grove et al. 2002). A large variation in isotopic composition is represented. Based on the available analyzed samples, the Shastina and Misery eruptive phases are characterized by low $^{87}Sr/^{86}Sr$ and high ε_{Nd} values. In the Sargents Ridge eruptive stage, only the high $^{87}Sr/^{86}Sr$ and low ε_{Nd} types are present in the analyzed andesites, but the other end member of the isotopic spread is represented in primitive basaltic andesites of Sargents Ridge age (95-15, Grove et al. 2002). The Hotlum phase of cone building also shows a wide variation in $^{87}Sr/^{86}Sr$ and ε_{Nd}. In contrast to the variability of the trace elements, the range in isotope values shown by the andesites and dacites compared to the primitive PMAs and BAs is roughly similar.

Petrography and mineral chemistry

Andesites and dacites are variably porphyritic and contain between 2 and 40 volume% phenocrysts, but most of the Shasta stratocone lavas contain between 20 and 30% phenocrysts (Table 4). Since all of the Shasta andesites and dacites show evidence of magma mixing phenocrysts are technically xenocrysts, but we will reserve the term xenocryst for mineral grains that have corroded and reacted textures. Plagioclase is the dominant phenocryst in lavas from the Sargents, Misery and Hotlum eruptive stages and constitutes $>70\%$ of the phenocryst volume. Plagioclase phenocrysts are tabular, subhedral and range from 0.5 to 5 mm in longest dimension, with <1 to 3 mm being the typical size range found in the lavas. Orthopyroxene, the next most abundant phenocryst phase in the Sargents, Misery and Hotlum lavas, is equant, elongate to irregular in shape and 1–1.5 mm in length. Augite

Table 2 Trace element analyses of andesite and dacite lavas from Mt. Shasta region

	Sr	Ba	Ce	La	Ga	Nb	Rb	Y	Zr	Zn	Cu	Cr	Ni
Hotlum													
82-91a	960	307	22	12	22	2	24	11	125	48	27	72	52
82-91b	1,039	282	20	12	22	3	20	11	123	46	14	85	61
82-96	861	305	17	10	22	3	27	13	121	46	29	50	37
82-97	611	409	22	13	26	3	40	10	136	49	16	58	13
83-44	714	354	23	15	24	3	26	11	110	73	26	68	40
83-45	666	364	21	15	27	3	31	8	97	69	39	27	25
83-46	557	385	22	13	24	4	29	12	105	73	23	33	23
83-54	617	430	23	14	23	4	41	8	120	70	18	53	17
83-55	668	392	18	14	23	3	36	11	115	72	33	63	18
97-4	682	355				–	33	11	119	56	26		25
97-5	989	392				–	37	9	126	63	48		44
97-6	994	387				–	35	11	132	66	41		50
99-12A	566	204	17			3	18	10	69			213	28
99-12B	517	198	15			3	14	12	53			108	43
99-13	697	350	27			5	29	12	113			59	33
99-14	767	333	25			6	29	12	114			51	39
99-15	996	403	36			5	27	13	121			43	44
99-16	1,000	394	29			5	26	13	123			50	49
99-17	850	304	25			5	27	12	108			43	36
99-18	1,020	407	32			5	26	12	122			51	50
99-19	1,060	260	24			4	19	9	103			46	52
Shastina													
82-82	1,147	308	24	14	23	3	23	13	150	51	45	66	55
83-53	933	320	21	18	26	3	22	12	124	71	45	94	67
83-50	987	328	27	15	26	3	23	11	128	71	46	76	65
83-52	1,014	329	24	16	25	3	22	12	129	71	56	74	49
83-51	1,010	330	21	17	25	3	21	10	127	68	38	72	69
83-57	1,129	222	18	13	26	1	15	9	87	61	20	41	62
83-58	1,157	282	22	16	27	2	20	10	114	67	42	41	53
85-3	1,138	308	34	17	19	5	16	13	96	51	61	94	53
95-13	1,120	208				1			71	47		82	49
95-12c													
96-1	1,050	293				–	32	9	117	60	66		47
96-5	1,160	211				–	30	–	101	52	26		35
96-7						–		–					
96-10b	1,080	211					34		117	68	43		59
96-11b													
96-12	1,100	218				–	29	–	95	53	28		42
96-13	1,090	222				–	27	–	109	52	25		42
97-3	1,910	1,170				–	56	13	182	65	55		53
97-7	1,030	325				–	31	11	137	63	55		53
99-4	1,860	1,110	63			6	28	12	156	65	49	89	94
99-5	1,100	293	30			5	20	12	114	53	46	37	57
99-6	1,250	344	46			5	20	13	145	74	38	99	55
99-7	1,040	297	27			5	19	10	116	50	55	63	45
99-10	808	272	16	10	20	3	18	8	93	44	20	8	13
99-11	1,040	305	28	14	21	5	21	11	121	54	46	47	52
Misery													
82-94d	1,293	414	33	18	26	2	22	15	164	56	46	30	24
82-99	806	416	18	15	21	3	29	14	131	57	31	47	21
82-93	589	384	19	11	22	4	35	14	131	60	29	45	16
82-98	625	416	17	14	21	4	40	20	136	63	23	52	13
82-101	709	299	19	10	21	2	29	12	121	48	53	15	9
82-100	745	379	16	9	22	3	22	11	116	43	16	10	9
82-103	737	337	20	10	22	3	31	15	120	60	27	44	16
82-104	706	306	17	10	22	3	30	12	122	49	17	16	7
82-105	831	322	18	11	22	2	25	13	117	53	47	36	34
83-49	939	334	23	18	26	3	23	11	127	68	41	75	64
83-56	763	309	18	14	26	2	29	7	103	64	29	13	15
83-59	700	311	14	13	28	3	29	8	107	63	28	16	15
85-2a	1,062	306	31	17	21	4	25	12	91	45	27	53	21
85-2b	1,050	306	29	16	21	4	22	11	96	42	22	56	23
85-48b	1,478	211	35	17	18	4	14	11	82	48	41	68	24
99-9	482	443	33	18	19	5	53	12	119	59	39	43	44

Table 2 (Contd.)

	Sr	Ba	Ce	La	Ga	Nb	Rb	Y	Zr	Zn	Cu	Cr	Ni
Sargents													
82-83	651	430	21	14	23	4	37	14	133	57	30	32	24
82-84a	515	513	31	19	22	5	64	15	163	50	7	64	14
82-85	903	628	41	27	21	6	41	13	190	64	40	77	59
82-86	781	365	19	12	21	4	29	14	130	58	20	53	24
82-87	893	291	13	11	23	2	22	11	111	53	27	33	37
82-88b	913	635	36	24	21	5	45	12	167	57	30	33	29
82-89	872	314	17	11	23	3	25	11	118	56	27	37	35
82-92a	478	475	24	14	22	4	56	11	138	50	15	19	11
82-95	487	512	31	20	20	6	70	18	170	52	21	73	31
82-102	806	322	19	13	22	3	30	15	122	55	27	69	18
85-55	973	586	46	26	17	5	21	15	121	58		122	47
85-56	976	591	52	26	17	4	20	15	118	63		130	51
85-57b	864	507	38	22	17	5	23	14	113	56		113	45
85-58	703	490	40	22	18	5	33	18	123	59		85	37
85-59	995	693	57	30	18	8	36	14	143	69		94	75
75-22													
85-42	381	808	52	115	27	9	42	44	239	69		2	–
85-43	249	693	43	25	20	8	65	22	191	44		–	–

Analyses were performed at two locations, LaTrobe University or U.S. Geological Survey. See Table 1 for location of analysis. Concentrations are in ppm. Dash indicates element was below detection limit. Blank space indicates element not analyzed

phenocrysts in these lavas are subhedral, equant and <1 mm in longest dimension. Although relatively less abundant, amphibole, olivine, ilmenite/magnetite and quartz are also present as phenocrysts or xenocrysts. Amphibole crystals are equant, elongate and range from <0.5 to ~ 2 mm in length. Olivine, ilmenite/magnetite and quartz fall in the size range of 0.1–1 mm. Quartz and olivine crystals commonly have irregular or cuspate outer margins. Olivine is also overgrown by orthopyroxene or amphibole. Crystals of ilmenite/magnetite are subhedral, range from 0.3 to 0.8 mm in longest dimension and commonly consist of distinct grains that share a common interface. Lavas with low phenocryst content were erupted during the Shastina stage of stratocone building and the majority of these lavas contain between 3 and 5% phenocrysts (either orthopyroxene or amphibole are the dominant phenocryst phases, Table 4). Highly porphyritic lavas with plagioclase as the dominant phenocryst phase were also erupted (Table 4), but are volumetrically less abundant in the Shastina eruptive phase. Some Shastina dacites contain olivine, orthopyroxene, augite glomerocrysts that are enclosed in magnesian amphibole phenocrysts (Table 4). Hotlum and Sargents Ridge andesite and dacite lavas also contain these mafic phenocrysts/xenocrysts assemblages. The phenocrysts from all four eruptive stages are set in a fine-grained hyalopilitic to pilotaxitic groundmass that consists of plagioclase laths, granular pyroxenes, oxides and glass.

A variety of silicic to ultramafic inclusions are present in the Mt. Shasta andesite and dacite lavas. Rare cm-sized granitic and metasedimentary inclusions have been found in all eruptive stages. Mafic igneous inclusions are also present in all phases of the stratocone. Textures of the mafic inclusions range from intersertal to gabbroic to granoblastic. Inclusions range in size from centimeters to decimeters, and samples range from aphanitic to inclusions with grain sizes of 1–5 mm. Intersertal- and gabbroic-textured inclusions contain a glassy, vesicular groundmass, and plagioclase, orthopyroxene, augite, oxides, $\pm$ olivine, $\pm$ amphibole are the constituent minerals. Mineral compositions indicate that these mafic inclusions are either quenched mafic magmas or cumulates derived from more primitive liquids. Samples 99-12A and 99-12B represent analyses of this cognate magmatic inclusion type (Tables 1, 2), and they are similar in texture and mineralogy to those found in lavas of Medicine Lake volcano to the east (Grove et al. 1997). Rare cm-sized inclusions of peridotite have been found in all eruptive phases, as well as orthopyroxenite inclusions that appear to record progressive metamorphism of serpentinite. These xenoliths are assumed to come from the underlying Trinity ultramafic complex.

Mineral compositional variation

A broad range of phenocryst compositions and a polymodal distribution in core compositions are characteristic of all Mt. Shasta andesites and dacites. Representative compositions are reported in Table 3. Plagioclase phenocrysts exhibit oscillatory zoning (Fig. 6e, f) and have core compositions in the range An_{28} to An_{88}. The range of plagioclase core compositions found in the Shastina and Misery Hill stage lavas is shown in Fig. 7. Plagioclase core compositions from Sargents Ridge and Hotlum stage lavas (Fig. 8) are similar to those of the Misery Hill lavas. Plagioclase core compositions display two major peaks in Misery Hill and Hotlum lavas at $An_{40\text{-}50}$ and $An_{55\text{-}70}$. The Sargents Ridge lavas show a major peak at $An_{40\text{-}50}$ and the

Table 3 Compositions of minerals in Mt. Shasta andesite, dacite and rhyodacite lavas

Sample no.	Mineral	SiO_2	TiO_2	Al_2O_3	Cr_2O_3	FeO	MnO	MgO	CaO	Na_2O	K_2O	Sum	Mg# or An
82-85													
pc	Opx	52.3	0.18	0.79	0.03	24.1	0.55	21.3	1.07	0.02		100.4	0.612
pc	Opx	55.6	0.05	2.84	0.42	7.27	0.19	33.8	0.98	0.02		100.6	0.892
pc	Cpx	52.9	0.53	2.04	0.53	5.17	0.14	17.97	20.6			99.9	0.861
pc	Oliv	40.2				9.94	0.17	50.7	0.06			101.1	0.901
pc	Plag	58.1		26.6		0.29		0.0	8.36	6.96	0.33	100.6	0.392
pc	Plag	54.2		29.3		0.29		0.03	11.2	4.72	0.22	99.9	0.560
82-91a													
ig	Ilm	0.06	42.2	0.11	0.04	53.9	0.38	1.56	0.0			98.3	
ig	Sp	0.16	12.5	0.89	0.40	81.6	0.29	1.11	0.0			97.1	
pc	Plag	51.3		30.4		0.49		0.09	13.1	3.84	0.09	99.3	0.650
pc	Opx	56.3	0.08	1.05	0.34	8.51	0.18	32.5	1.05	0.0		100.0	0.871
pc	Cpx	53.1	0.27	1.78	0.43	4.25	0.08	17.0	22.3	0.30		99.5	0.876
pc	Opx	52.3	0.27	0.88	0.04	25.1	0.55	22.3	1.11	0.0		100.0	0.638
pc	Plag	60.8		25.1		0.10		0.0	6.62	7.42	0.61	100.7	0.319
83-53													
pc	Opx	56.6	0.09	1.50	0.51	7.99	0.17	33.6	0.81	0.02		101.2	0.882
ig	Cr-Sp	0.0	0.92	12.6	44.6	29.0	0.34	12.6	0.0			98.9	
pc	Plag	50.1		31.3		0.50		0.03	14.5	3.14	0.10	99.7	0.714
82-82													
pc	Cpx	53.5	0.14	1.62	0.68	3.82	0.07	18.1	22.4	0.25		100.6	0.894
82-84a													
pc	Cpx	54.4	0.17	1.27	0.79	3.22	0.09	18.9	22.0	0.21		101.3	0.913
pc	Plag	62.2		24.1		0.16		0.0	6.09	7.65	0.79	101.1	0.292
pc	Oliv	39.5		0.02	0.06	21.3	0.31	41.5	0.06			102.4	0.777
pc	Plag	49.5		31.6		0.25		0.05	15.0	3.20	0.13	99.7	0.716
pc	Amph	42.5	3.18	12.0	0.0	13.9	0.14	13.6	10.9	2.95	0.44	99.5	0.636
pc	Opx	52.7	0.26	0.49	0.0	22.2	0.68	23.4	1.54			101.2	0.653
82-98													
ig	Ilm	0.10	48.9	0.15	0.0	49.0	0.50	2.00	0.02			100.8	
ig	Sp	0.23	17.8	1.43	0.09	75.2	0.40	1.25	0.0			96.5	
McKenzie Butte 75-SH22													
pc	Plag	59.4		25.3		0.21		0.03	7.29	7.17	0.31	99.8	0.353
pc	Opx	51.0	0.11	0.39	0.0	28.4	1.08	17.1	0.93	0.0		99.0	0.518
pc	Amph	42.0	2.40	9.93	0.0	18.7	0.36	10.4	10.3	2.30	0.42	96.8	0.497
ig	Sp	0.22	13.0	1.94	0.05	79.7	0.53	0.80	0.06			96.3	
ig	Ilm	0.07	48.4	0.15	0.0	48.4	1.00	1.15	0.05			99.3	

Plag plagioclase, *Opx* orthopyroxene, *Cpx* augite, *Oliv* olivine, *Amph* amphibole, *Sp* spinel, *Cr-sp* chrome spinel, *Ilm* ilmenite, *pc* phenocryst core, *ig* intergrowth

majority of the Shastina core compositions are in the range of An_{55-70}. Many plagioclase crystals contain sieve-textured interiors or regions of wormy melt inclusions. In individual whole rock samples both unreacted and sieve-textured phenocrysts are found to display similar compositional variations. Shastina lavas are distinct from all other eruptive stages in the predominance of the mid-An content population (An_{55-70}, Fig. 7).

Both Fe-rich and Mg-rich pyroxenes are present in the lavas of all four eruptive stages (Figs. 9, 10). Lavas of the Shastina eruptive stage contain a lower proportion of the Fe-rich augite and orthopyroxene compared to the lavas of the Hotlum and Sargents eruptive stages which have a higher proportion of the Fe-rich pyroxene population. Histograms of core compositions from all four eruptive stages generally display faintly to strongly bimodal compositions (Figs. 9, 10). Core compositions show peaks in distribution at Mg#s of 55-60, 65-70 and 80-84. High Mg# orthopyroxene crystals are overgrown by distinctive Fe-rich rims (Fig. 6c). High Fe orthopyroxene grains display distinct overgrowth rims of magnesian orthopyroxene and contain wormy internal Mg-rich reaction zones (Fig. 6d). Fe-rich orthopyroxene phenocrysts contain ilmenite and/or magnetite inclusions. Augite core compositions (Figs. 9, 10) range from Mg# of 91 to 65. Wollastonite (Wo) contents range from 38 to 46. Magnesian augite (Mg# 82-91) crystals are present as solitary grains (Fig. 6g) or as intergrowths with Mg-rich orthopyroxene (Fig. 6c). High Mg# augite crystals display hour-glass sector zoning with minor-element-depleted sectors developed parallel to the c crystallographic axis (Fig. 6g). The Fe-rich augites are reverse-zoned in Mg# and contain inclusions of ilmenite and/or magnetite.

Olivine phenocrysts range from Fo_{91} to Fo_{66} (Fig. 11b). Phenocryst textures vary from euhedral and normally zoned (Fig. 6a), to overgrown by orthopy-

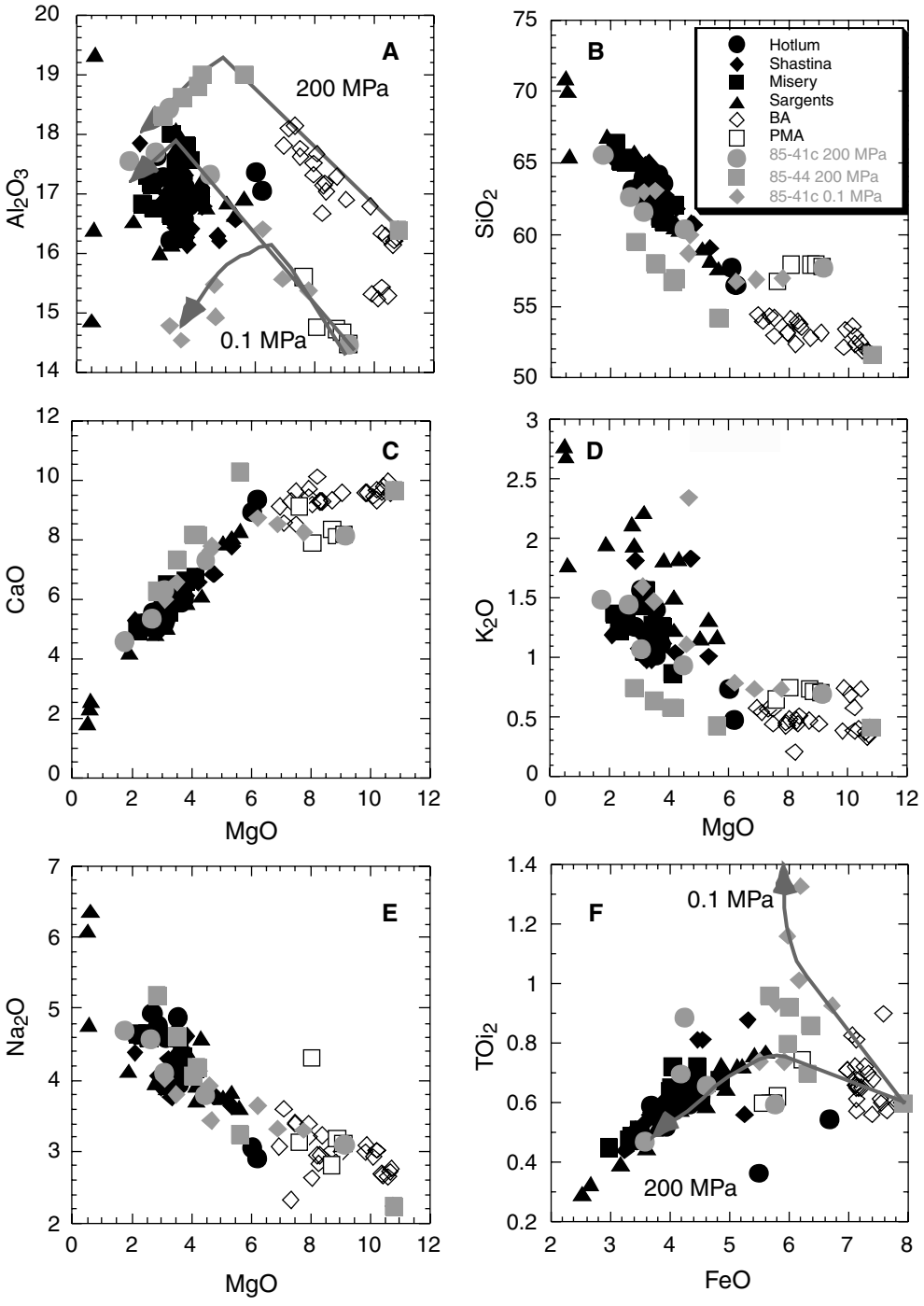

Fig. 3 Major element compositional variations in Mt. Shasta region lavas. Also shown are compositions of BA and PMA lavas and experimentally determined liquid lines of descent from 200 MPa, NNO buffered, H_2O-saturated crystallization experiments on 85-44 and 85-41c and 0.1 MPa QFM-buffered anhydrous experiments on 85-41c (Baker et al. 1994; Grove et al. 2002, 2003). *A* Al_2O_3 vs. MgO, *B* SiO_2 vs. MgO, *C* CaO vs. MgO, *D* K_2O vs. MgO, *E* Na_2O vs. MgO and *F* TiO_2 vs. FeO All oxides are in wt.%

roxene (Fig. 6b) or surrounded by a scalloped or cuspate outer margin. Amphibole phenocrysts span a range of Mg# from 83 to 58 (Fig. 11a). Most crystals are normally zoned, but some are reverse zoned in Mg# or exhibit oscillatory zoning. The more magnesian amphibole crystals enclose Mg-rich olivine and pyroxene. Amphibole with Mg# <75 contains plagioclase as an inclusion phase. Amphibole crystals show a range of decompression-breakdown textures from thin, micron-sized, overgrowths to coarser-grained rims of spinel + plagioclase + pyroxene (Fig. 6h). Magnesian amphibole crystals always have thin breakdown rims (<10 micron, see Grove et al. 2003, Fig. 9). Compositions of coexisting ilmenite-hematite and ulvöspinel-magnetite phenocrysts were used to estimate oxygen fugacity and temperature (Fig. 12a). The method outlined in Anderson and Lindsley (1988) shows temperature and oxygen fugacity (fO_2) of crystallization relative to the NNO (Nickel—Nickel Oxide) buffer. Oxygen fugacity shows a wide range from ~NNO-1 to NNO + 1 and there is no systematic relation between fO_2 and eruptive stage.

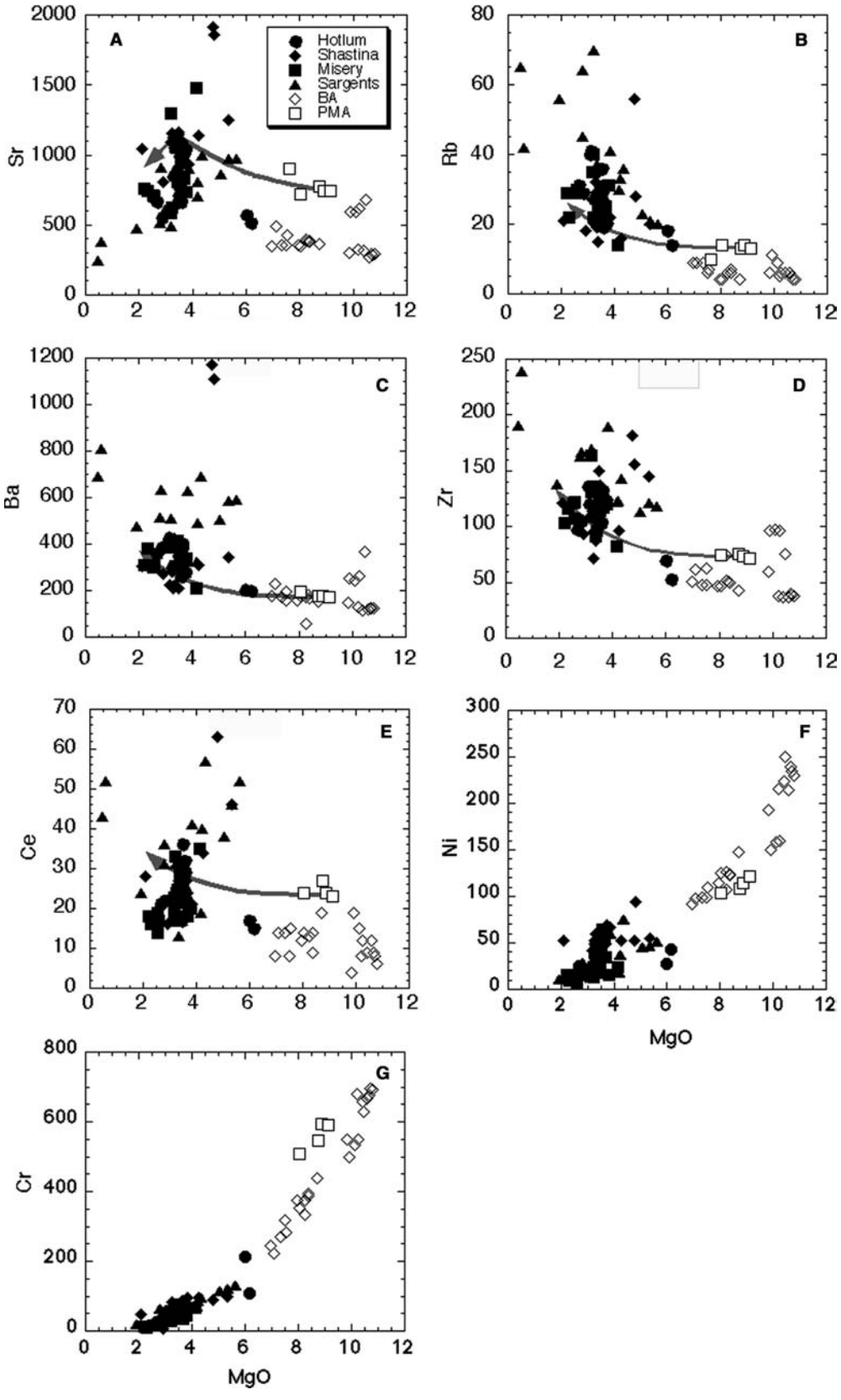

Fig. 4 Trace element compositional variations of Mt. Shasta region lavas. The *gray curve with the arrow* shows a calculated fractional crystallization path. Fractionation model starts from PMA 85-41b (see Tables 5, 6). *A* Sr vs. MgO, *B* Rb vs. MgO, *C* Ba vs. MgO, *D* Zr vs. MgO and *E* Ce vs. MgO. *F* Ni vs. MgO and *G* Cr vs. MgO. Trace elements in ppm, MgO in wt.%

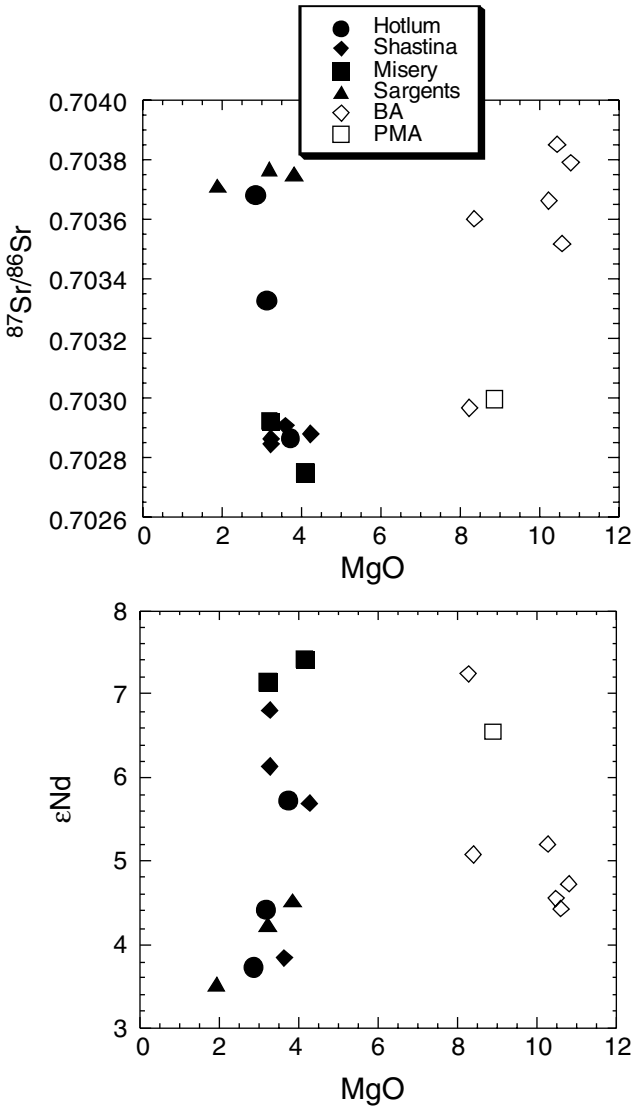

Fig. 5 Sr and Nd isotopic compositional variations in Mt. Shasta region lavas as a function of wt.% MgO. Data are from Grove et al. (2002)

Table 4 Modal phase proportions in Mt. Shasta andesites and dacites

Sample	SiO_2 (%)	Phenocrysts[a]						Groundmass
		Plag[c]	Opx	Cpx	Amph	Ilm/Mt	Oliv	
Hotlum								
82-91a	63.5	12.8/ 11.9	3.9	2.4		< 1		68.9
82-96	63.2	18.1/ 6.8	1.4	1.6		< 1		69.0
82-97	64.1	14.6/ 7.2	3.8	1.8	tr		< 1	70.4
83-46	63.0	16.6/ 7.7	1.1	< 1		< 1		70.5
83-54[b]	64.2	13.0/ 7.2	5.2	3.4	< 1	< 1		70.0
Shastina								
82-82	62.8	-/0.6	2.0	1.3				96.1
83-50	63.4	-/18.1	2.2	2.1				77.6
83-51	62.8	-/13.4					4.8[d]	81.8
83-52	63.4	-/17.4					4.8[d]	77.8
83-53	63.4	-/20.6	3.4	2.0				73.9
83-57	64.5	-/11.9		< 1	7.8[e]			80.0
83-58	64.2	-/0.4					2.5[d]	97.1
85-3	62.0	-/17.3	3.9	3.0				75.8
96-5	63.8	-/12.3		< 1	7.1[e]			79.8
Misery								
82-98[b]	63.8	13.2/ 7.1	3.8	2.1	< 1			73.6
82-101	65.1	3.2 /16.5	4.1	1.4		tr		74.9
82-103	60.9	20.6/ 13.5	6.6	2.6		< 1	tr	56.5
82-104	65.0	3.0 / 19.2	4.0	2.3				71.5
82-105[b]	61.3	17.4/ 11.4	4.8	2.4		< 1		63.9
83-49	63.6	2.6 / 15.6	2.6	2.7		< 1		76.3
85-2b	62.9	10.1/ 8.0	3.9	3.1				74.9
Sargents								
82-83	61.8	25.0/ 9.0	5.7	1.5		< 1	tr	58.5
82-84a[b]	65.8	16.0/ 3.1	1.7	1.6	6.3	< 1	< 1	72.3
82-85	61.5	11.4/ 4.0	2.7	1.0	5.1	< 1	< 1	74.7
82-87[b]	61.9	10.8/ 17.6	4.0	2.4		< 1		64.9
82-88b	63.5	13.4/ 5.6	2.5	0.8	6.0	1.0		70.2
82-89	61.6	6.5/ 10.4	2.4	1.4			tr	79.3
82-95[b]	64.4	15.5/ 8.3	2.5	1.4		< 1	< 1	71.2
82-102[b]	60.9	15.8/ 12.3	4.8	2.8		< 1		63.8
85-55	58.3	3.4 / 1.3	1.7	6.5			2.0	85.1
85-56	57.6	4.4 / 1.1	2.8	7.7			1.6	82.3

[a]Volume % (vesicle free) calculated from 1,000 to 1,100 points per thin section. For the Hotlum, Misery and Sargents samples, phenocrysts were grains ≥0.05 mm in longest dimension; for the Shastina samples phenocrysts were grains ≥0.1 mm in longest dimension. Abbreviations: *Plag* plagioclase, *Opx* orthopyroxene, *Cpx* clinopyroxene, *Amph* amphibole, *Ilm*/*Mt* ilmenite/magnetite, *Oliv* olivine. tr indicates present in proportions < < 1 vol %.
[b]Quartz is also present as a xenocryst
[c]For plagioclase from the Hotlum, Misery and Sargents eruptive stages the first value refers to phenocrysts ≥0.5 mm in longest dimension and second value refers to crystals between 0.05 and 0.5 in longest dimension. For the Shastina lavas plagioclase size ranges are > 1 mm and between 0.1 and 1 mm in longest dimension; dash indicates that no large plagioclases were observed
[d]In these samples the value in the olivine column refers to sum of all mafic phenocrysts (oliv + opx + cpx)
[e]In these samples amphibole phenocrysts surround oliv + opx + cpx grains

Discussion

Origin of compositional variability in Shasta stratocone lavas

Major elements

There are two primitive mafic lava types at Mt. Shasta (BA and PMA) that contain the same phenocryst assemblage that represents the mafic compositional end member in the mixed stratocone lavas. These primitive mafic lavas erupted from flank vents around the Shasta edifice. The results of experimental investigations (Grove et al. 2003) on these lavas will be used to place limits on the conditions of fractional crystallization. Residual liquids from isothermal experiments on primitive Mt. Shasta region lavas (BA, 85-44 and PMA, 85-41c) provide an adequate approximation of fractional crystallization paths when the fraction of liquid is high (> 40 wt.%, see Table 5), and these experimental liquids are plotted in Figs. 1a and 3 along with Shasta lava compositions. Figure 1a shows compositions of liquids from experiments performed at 200 MPa under H_2O saturated conditions at the NNO buffer. Figure 3 shows the results of 200 MPa NNO H_2O-saturated experi-

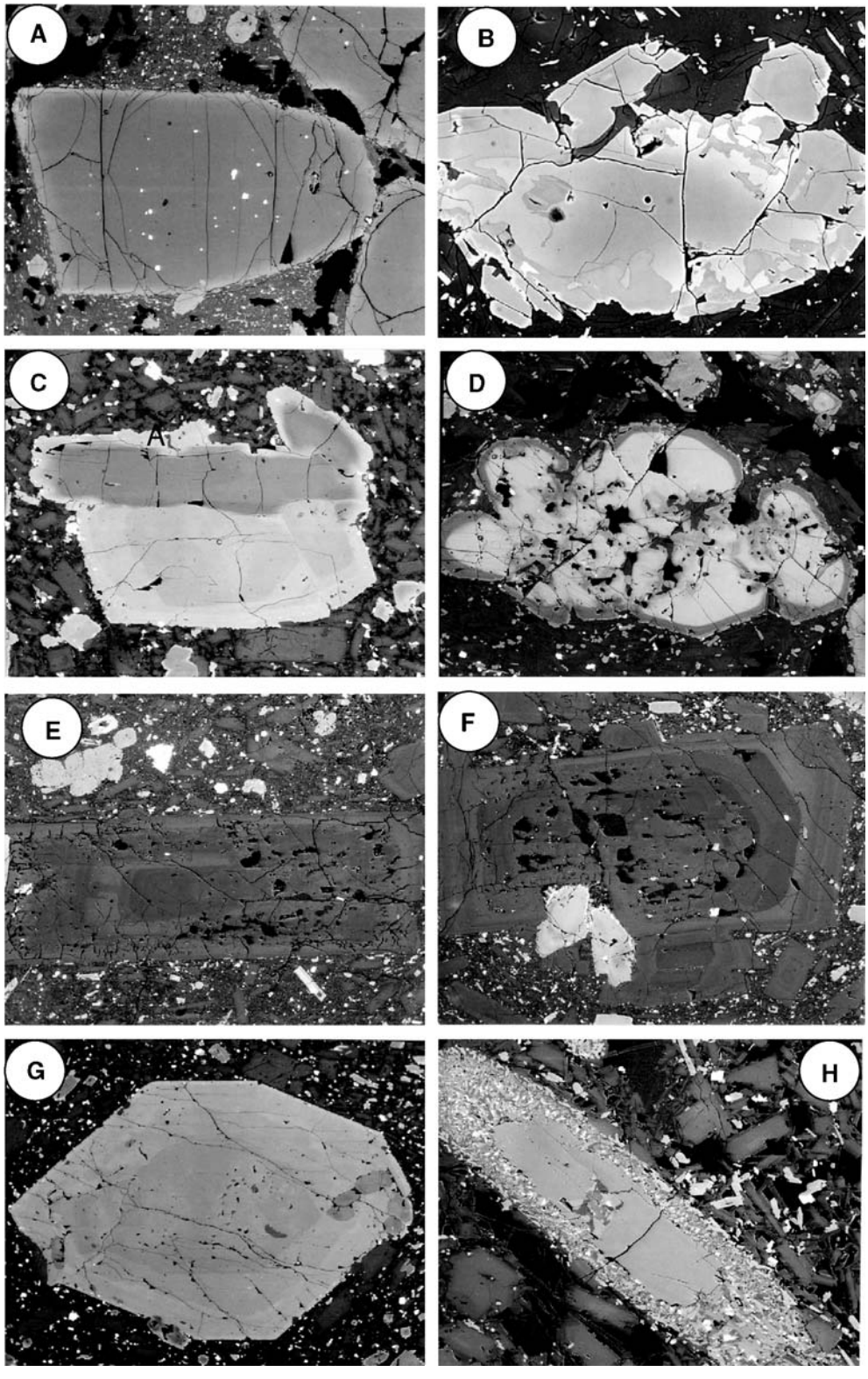

Fig. 6 Phenocryst textures of Mt. Shasta region andesites and dacites. Back-scattered electron images have a horizontal width of 0.25 mm unless otherwise noted. See Table 4 for mineral core compositions. **a** Fo_{90} olivine with Cr-spinel inclusions in Sargents andesite 85-57. **b** $Fo_{70\text{-}75}$ olivine core and Fe-rich rim overgrown by orthopyroxene in Misery andesite 82-103. **c** Magnesian augite and orthopyroxene intergrown as glomerocrysts in Misery andesite 85-48b. Image width = 0.1 mm. Both augite and orthopyroxene are surrounded by distinctive Fe-rich overgrowth rims. **d** Fe-rich orthopyroxene overgrown by Mg-rich rim shows complex resorption/reaction texture, a characteristic of melt/xenocryst reaction; Sargents andesite 85-57. **e** Oscillatory zoned plagioclase phenocryst containing Ca-rich core ($\sim An_{70}$) in Misery andesite 85-48b. **f** Oscillatory zoned plagioclase phenocryst containing Na-rich core ($\sim An_{40}$) in Sargents andesite 82-102. **g** Mg-rich augite (Mg# ~90) in Misery andesite (85-48b). Outer, normally zoned exterior includes Mg-rich orthopyroxene (Mg# ~87). **h** Reacted amphibole phenocryst in Shastina dacite 83-57. Image width = 1.25 mm. Interior of crystal contains plagioclase and orthopyroxene. Exterior rim consists of pyroxene + spinel + plagioclase reaction assemblage

ments on BA and PMA and experiments performed on the PMA composition at 0.1 MPa anhydrous at the QFM (Quartz-Fayalite-Magnetite) buffer (see Grove et al. 2003). The closest match of the trend defined by the Shasta stratocone andesites and dacites on the FeO*/MgO vs. SiO_2 diagram is with the results of the PMA experiments H_2O-saturated at 200 MPa. Two Hotlum samples lie above the PMA trend at low SiO_2 and are distinguishable in Fig. 3. These are samples 99-12A&B which are quenched magmatic inclusions that may have lost interstitial melt by gas-driven filter pressing (Sisson and Bacon 1999). The three Sargents samples that also

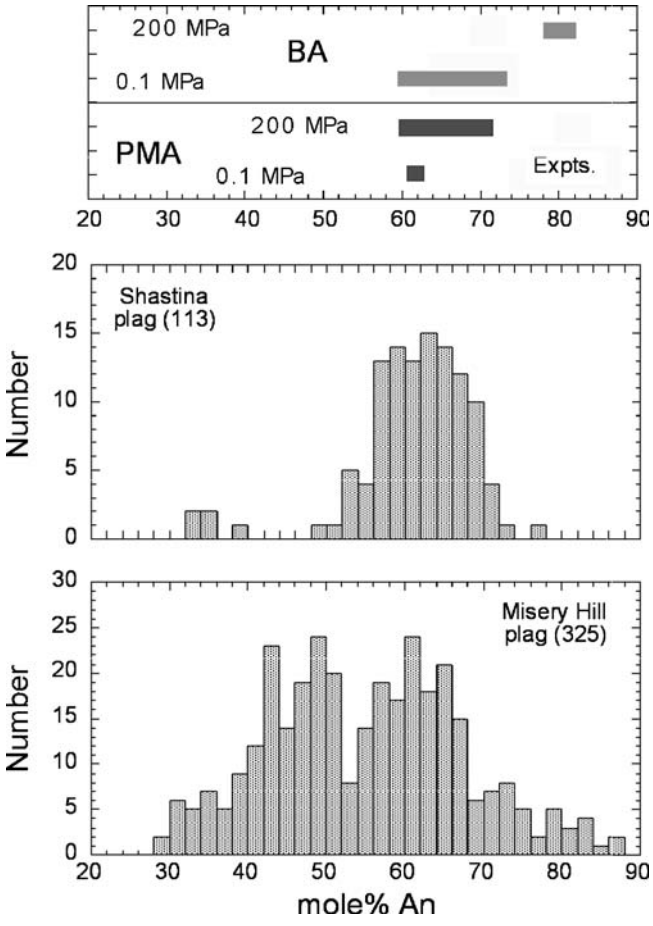

Fig. 7 Variation in plagioclase phenocryst core compositions of andesites and dacites from the Shastina and Misery eruptive stages and compositional range of plagioclase produced in experiments on primitive lavas. Top panel shows compositional range of plagioclase produced in 200 MPa, H_2O-saturated and 0.1 MPa anhydrous crystallization experiments on PMA 85-41c and BA 85-44 (Data from Grove et al. 2003). Horizontal axis in all panels is mole% anorthite. *Middle panel* shows histogram of phenocryst core compositions of plagioclase from Shastina lavas and the lower panel shows core compositions from the Misery Hill eruptive stage. Numbers in parentheses are the number of analyses used in each histogram

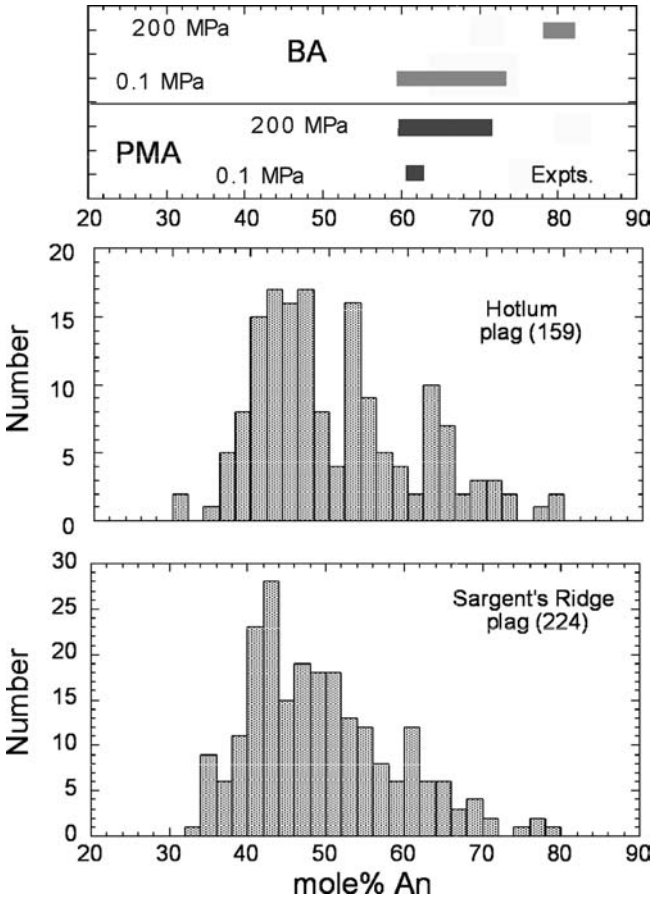

Fig. 8 Variation in plagioclase phenocryst core composition of andesites and dacites from the Hotlum and Sargents eruptive stages and compositional range of plagioclase produced in experiments on primitive lavas as shown in Fig. 7

lie above the PMA trend in Fig. 1a are the mafic end members of the Panther Creek Flow, a compositionally zoned mixed andesite (samples 85-55, −56, −57 and −58). The main group of stratocone lavas lies on or below the trend defined by the PMA liquid line of descent at 200 MPa. The Shasta andesite and dacite lavas are mixed magmas. Although the experiments provide a guide to fractionation conditions, the lavas would not be expected to plot directly on a fractional crystallization path, especially if the crystallization paths contain kinks or curves, as observed in Fig. 3 for all elements.

The liquid line of descent defined by the PMA 200 MPa NNO experiments extends into and most closely tracks the array of stratocone andesite and dacite lavas. In contrast, the trend defined by the 200 MPa BA experiments does not pass through the composition space defined by the lavas. The mismatch between BA experimental trends and the data for stratocone lavas is greatest in the $MgO–Al_2O_3$, $MgO–SiO_2$ and $MgO–K_2O$ variation diagrams. Note that on the $MgO–Al_2O_3$, $MgO–SiO_2$ and $MgO–K_2O$ plots (Fig. 3a, b, d) a series of BA lavas from a flank vent (Cinder Cone, Baker et al. 1994) define a trend that parallels the 200 MPa trend and is separate from the stratocone trend, suggesting a different fractionation process. Baker et al. (1994) investigated the petrology of the evolved Cinder Cone lavas and found evidence for fractional crystallization of a magma with 4–6 wt.% H_2O consistent with crystallization between ~100 and 200 MPa, H_2O-saturated.

The $FeO–TiO_2$ diagram (Fig. 3f) compares the lava compositions with the 200 and 0.1 MPa liquid lines of descent. The low pressure, anhydrous crystallization trend diverges dramatically from the compositional fields defined by the lavas, while the 200 MPa (~6 wt.% H_2O at saturation) trend passes through the data array for the Shasta lavas.

Variations in $MgO–Al_2O_3$ (Fig. 3a) are the most sensitive indicator of variations in water content, and are a reflection of the influence of H_2O on plagioclase appearance temperature. In the 200 MPa experiments,

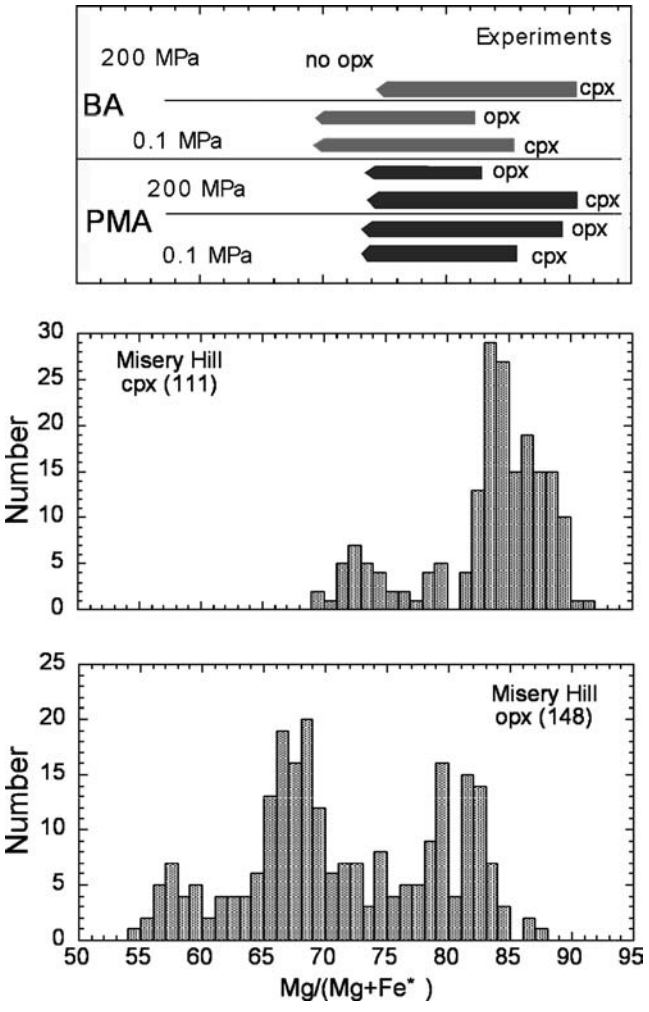

Fig. 9 Variation in phenocryst core composition found in orthopyroxene (*opx*) and augite (*cpx*) of andesites and dacites from the Misery eruptive stage and compositional range of opx and cpx produced in experiments on primitive lavas. Top panel shows compositional range of orthopyroxene and augite produced in 200 MPa, H_2O-saturated and 0.1 MPa anhydrous crystallization experiments on BA 85-44 and PMA 85-41c (Data from Grove et al. 2003). Horizontal axis in all panels is ($Mg\# = 100*Mg/(Mg + Fe^*)$ where all Fe was assumed to be Fe^{2+}). *Middle panel* shows histogram of phenocryst core compositions of cpx and *lower panel* shows opx core compositions from the Misery Hill eruptive stage. Numbers in parentheses are the number of analyses used in each histogram

the residual PMA liquid reaches ~18 wt.% Al_2O_3 and 3 wt.% MgO before plagioclase appears and causes a decrease in Al_2O_3 with increasing differentiation. At 0.1 MPa anhydrous conditions plagioclase appears earlier in the crystallization sequence and the maximum Al_2O_3 content (~16 wt.%) occurs at 6.5 wt.% MgO. At 100 MPa H_2O saturated conditions the maximum would occur at ~17 wt.% Al_2O_3 where MgO content is ~4 wt.% (Grove et al. 1997). The 100 and 200 MPa Al_2O_3 peaks would, therefore, bracket most of the Shasta andesite compositions on the plot. Thus, a range of H_2O-saturated conditions from 100 to 200 MPa is permissible, which translates into 4–6 wt.% H_2O; a range similar to that inferred by Anderson (1979), Sisson and Grove (1993) and Baker et al. (1994) for Shasta-region lavas. Water content provides only a minimum estimate on the pressure of crystallization. It is also possible that the Shasta lavas were H_2O-undersaturated or saturated with a mixed volatile fluid (H_2O-CO_2-S-Cl), which is the case for many subduction-related volcanic systems (Symonds et al. 1994). This would render any H_2O-based estimate of depth a minimum value. If the liquid is vapor-saturated with H_2O, a pressure of 200 MPa implies a depth of 7.4 km for average continental crust ($\rho = 2.7$ g cm^{-3}) or 9 km if the overburden is mostly volcanic rock ($\rho = 2.2$ g cm^{-3}).

Mineral compositional variations in lavas

The textures (Fig. 6) and multiple populations of phenocryst core compositions (Figs. 7, 8, 9, 10, 11) indicate that magma mixing has played an important role in the origin of the stratocone lavas. The phenocryst mineral compositions can be used to provide estimates of the crystallization conditions and of the compositions of the end members of magma mixing. Variations in H_2O content and pressure change the phase appearance sequence and phase appearance temperatures (Grove et al. 2003), which in turn changes the compositions of the minerals that crystallize.

Mafic inputs—crystallization conditions

Olivine, orthopyroxene, augite and amphibole with high Mg# are present in the Shasta andesite and dacite lavas, and this compositional information is used along with the mineral compositions produced in experiments on primitive BA and PMA liquids to identify the conditions and liquid compositions of the mafic end member(s) involved in the mixing processes.

Olivine preserved in the andesite and dacite lavas reaches a maximum of Fo content of 91% and the compositional distribution shows a broad peak from Fo_{84} to Fo_{88} (Fig. 11b). In the 200 MPa experiments on the BA and PMA, olivine is the liquidus phase and the most magnesian olivine in the Shasta stratocone lavas falls within the range of the liquidus BA and PMA olivine compositions ($Fo_{89\text{-}93.8}$). At high H_2O contents the first silicate mineral that crystallizes after olivine is augite. The composition of the coexisting augite and olivine can provide evidence of H_2O content. The population of augite phenocrysts in the Shasta lavas has a broad compositional peak that extends over the Mg# range of 90–83 (Figs. 9, 10). In the 200 MPa experiments the first clinopyroxene to crystallize has an Mg# of ~90 (Fig. 9) and would coexist with Fo_{87} olivine, which corresponds to a peak in the olivine composition frequency distribution (Fig. 11). Thus, we infer that one mafic end member of mixing was a liquid derived from a BA or PMA parent that had undergone a small amount of fractional crystallization (< 5% based on modeling of

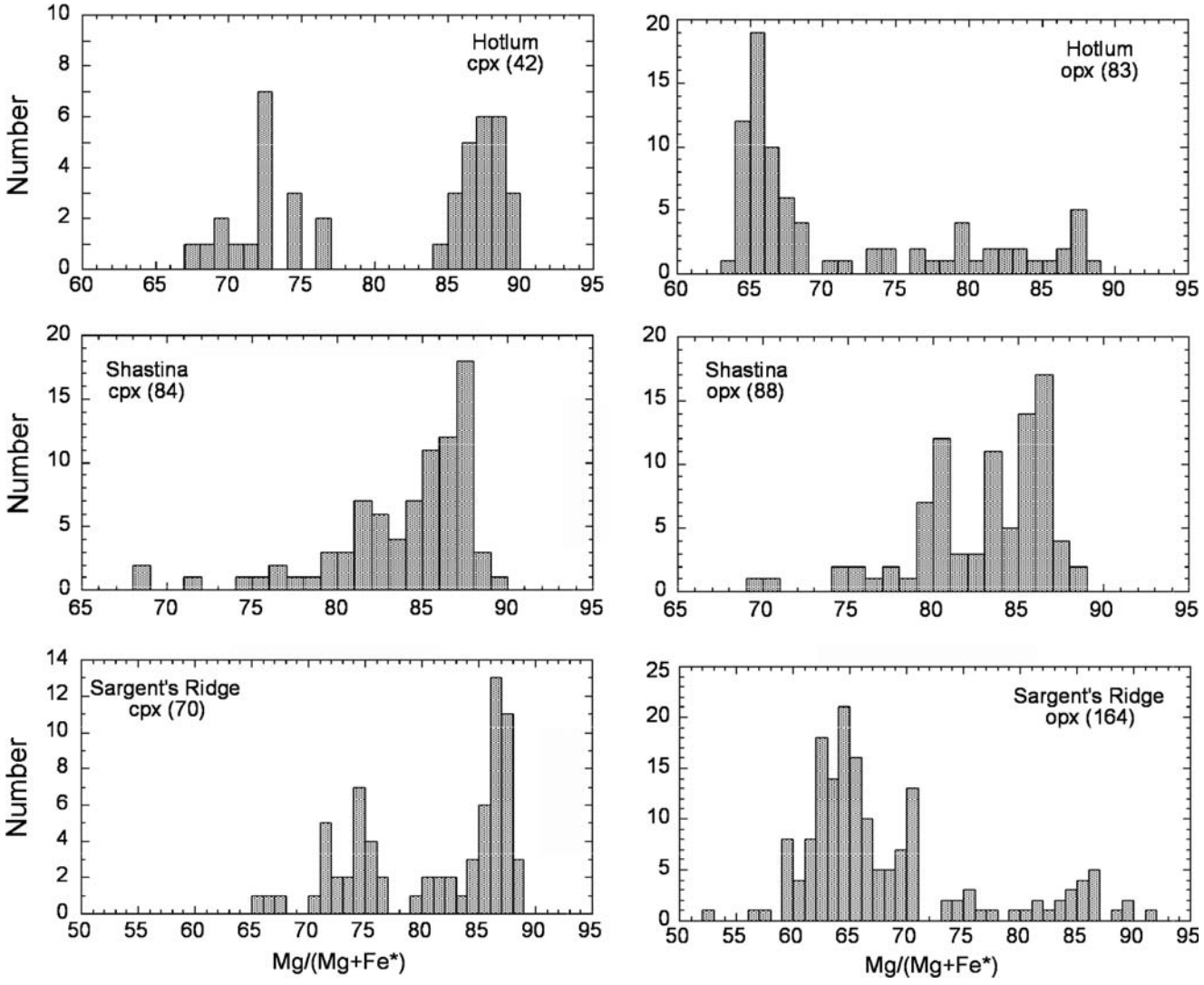

Fig. 10 Variation in phenocryst core composition found in opx and cpx of andesites and dacites from the Hotlum, Shastina and Sargents eruptive stages

experimental liquid lines of descent) at ≥200 MPa with a pre-eruptive H_2O content of ~6 wt.%.

The orthopyroxene phenocryst core compositions in Shasta lavas exhibit either two or three peaks in their Mg# frequency distribution (Figs. 9, 10) and the high Mg# peaks either approach or slightly exceed an Mg# of 85. Orthopyroxene appearance in the primitive BA and PMA compositions is H_2O-content (pressure) dependent. For the BA composition, orthopyroxene did not appear at the lowest temperature investigated at 200 MPa, and augite, olivine and amphibole were the saturating Fe, Mg phases. Orthopyroxene with an Mg# of 82 appeared as a crystallizing phase in the BA composition at 0.1 MPa, well below the observed maximum Mg# in the Shasta lavas. The Mg#s of the first orthopyroxene to appear in the PMA experiments were 90 at 0.1 MPa, and 82 at 200 MPa. The variation in orthopyroxene Mg# is caused by the influence of varying H_2O content; the olivine primary phase volume expands with increasing H_2O-saturated pressure, thereby suppressing orthopyroxene crystallization to lower temperature and decreasing its Mg#. Therefore, orthopyroxene Mg# can provide another estimate of pre-eruptive H_2O content. A peak of orthopyroxene at Mg# 85 corresponds to ~100 MPa, H_2O saturated conditions.

Augite and orthopyroxene coexist as glomerocrystic intergrowths (Fig. 6c), indicating coprecipitation. In the most Mg-rich coexisting pairs the orthopyroxene has an Mg# of 87 and the calculated 2-pyroxene temperature for the coexisting pair (82-91a Table 3) is ~1,000°C. This Mg# and temperature range require a minimum pressure of 70 MPa, if the temperature—pressure dependence of two-pyroxene saturation from the PMA experiments is interpolated from 0.1 to 200 MPa.

Amphibole phenocryst core compositions (Fig. 11a) also show a broad peak in their frequency distribution at an Mg# of 80 and they have a maximum Mg# of 83. Grove et al. (2003) investigated the significance of this high Mg# amphibole through a series of H_2O-saturated experiments carried out at 200 and 800 MPa on 85-44.

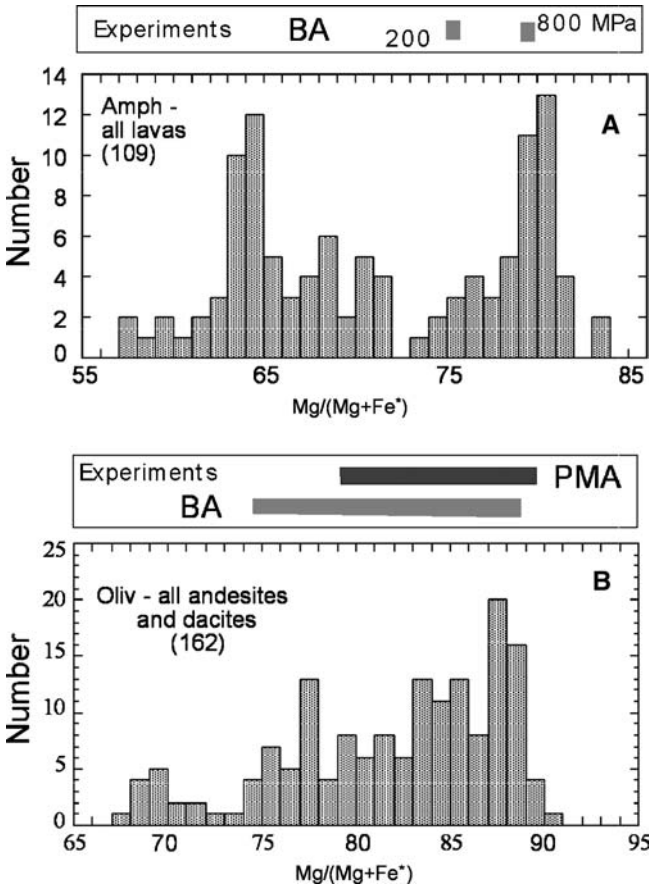

Fig. 11 Variation in phenocryst core compositions of amphibole (**a**) and olivine (**b**) from all Shasta region andesites and dacites. Horizontal axis in all panels is (Mg# = 100*Mg/(Mg + Fe*)). *Numbers in parentheses* are the number of analyses used in each histogram. Experimental amphiboles are from 200 and 800 MPa, H_2O-saturated experiments on 85-44. Experimental olivine compositions are from 200 MPa runs

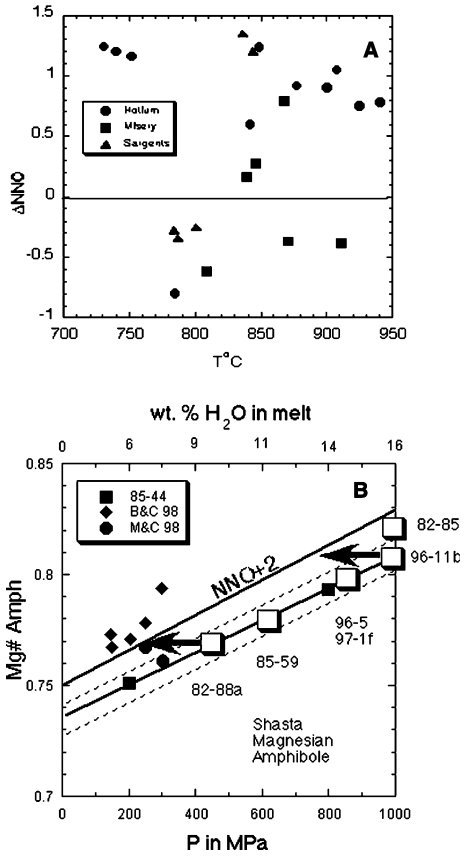

Fig. 12 **A** Log fO_2 relative to the Nickel—Nickel Oxide buffer ([*NNO*) vs. temperature plot for coexisting Fe-Ti oxide pairs from Shasta region andesites and dacites. Values on vertical axis indicate deviation of sample from the log fO_2 of NNO at the indicated temperature (Huebner and Sato 1970). **B** Mg# of first amphibole to appear in H_2O-saturated experiments on 85-44 at the NNO buffer at 200 and 800 MPa is plotted against pressure (*solid squares*) from Grove et al. (2003). *Upper scale* shows H_2O contents of H_2O-saturated liquids. A linear extrapolation was used by Grove et al. (2003) to infer pressure and H_2O content of amphibole crystallization. Also shown are experiments performed by Blatter and Carmichael (1998) on a high-SiO_2 andesite at NNO + 3 (*solid circles*) and from Moore and Carmichael (1998) at ~NNO + 1 and NNO + 2 (*solid diamonds*). A correction for the effect of increasing fO_2 on amphibole Mg# (NNO + 2) is also shown. *Large open squares* are compositions of high Mg# amphiboles in Shasta lavas. The high Mg# of amphibole in 82-85 and 96-11b indicate lower crustal pressures and high H_2O contents. Dashed boundary on either side of the Mg#—P line is the 2σ uncertainty of amphibole composition from Grove et al. (2003)

Amphibole with an Mg# of 79 becomes a near-liquidus phase at 800 MPa and appears after olivine and augite. In contrast, amphibole has an Mg# of 75 when it first appears as a crystallizing phase with plagioclase at 200 MPa (Fig. 12b). These H_2O-saturated experiments were performed at the NNO buffer, and amphibole stability depends on both melt H_2O content and fO_2 (in addition to other melt compositional variables; e.g., Sisson and Grove 1993). The maximum fO_2 from coexisting oxides (NNO + 1.4, Fig. 12a) can be used along with the experiments of Grove et al. (2003) at NNO, Blatter and Carmichael (1998) at NNO + 3.5, Moore and Carmichael (1998) at NNO + 2 and Grove and Juster (1989) at NNO + 2 to correct for the effects of co-variations in oxygen fugacity and H_2O-saturated pressure on amphibole Mg#. This correction is shown as the line labeled NNO + 2 in Fig. 12b. When this correction is applied the highest Mg# (83) amphibole found enclosing olivine and pyroxene requires an H_2O-saturated pressure > 900 MPa and the lower bound (Mg# 77) a pressure of 300 MPa (Fig. 12b). Magmatic H_2O contents of 15 wt.% are necessary to stabilize the Mg# = 83 assemblage at 900 MPa.

Plagioclase phenocryst core compositions in Shasta lavas contain several peaks in the An content frequency plot (Figs. 7, 8). In the Sargents, Misery and Hotlum stages of the stratocone the frequency distribution has a broad peak of high An from An_{55} to An_{70} that tails off to a maximum of An_{88}. In the Shastina stage this broad peak from An_{55} to An_{70} is the major feature of the frequency distribution. The plagioclase compositional variations produced in the PMA and BA experiments are quite distinct. At 200 MPa the first plagioclase to crystallize in

Table 5 Crystallization models that derive Shasta andesitic lavas

Fractionation model—major elements	SiO_2	TiO_2	Al_2O_3	FeO	MgO	CaO	Na_2O	K_2O	P_2O_5
Parent compositions									
PMA[a]	57.93	0.6	14.68	5.7	8.89	8.14	3.18	0.72	0.16
BA[b]	51.68	0.6	16.4	7.93	10.79	9.67	2.24	0.42	0.11
Major element abundances in fractionated melts of 85-41b									
Step 1[c]	60.73	0.71	18.07	5.26	3.42	7.12	3.95	0.9	0.2
Step 2[d]	65.11	0.72	17.48	3.33	2.01	5.26	4.58	1.24	0.28
Experimentally produced residual liquids, 200 MPa, H2O-saturated, NNO buffer (Grove et al. 2003)									
PMA, #9[e]	65.6	0.47	17.6	3.55	1.75	4.63	4.7	1.5	0.23
BA, #5[f]	59.5	0.96	18.3	5.68	2.86	6.27	5.2	0.75	0.23
Shasta region rhyodacite from McKenzie Butte (Table 1)									
75-22	70.08	0.33	16.4	2.66	0.54	2.35	4.79	2.69	0.1

F melt fraction, *plag* plagioclase, *opx* orthopyroxene, *cpx* augite, *oliv* olivine, *sp* spinel

[a]PMA = parent composition 85-41b (Baker et al. 1994; Grove et al. 2002)

[b]BA = parent composition 85-44

[c]Step 1, 0.42 oliv + 0.58 cpx, F = 1.0 to 0.8. The major element fractional crystallization model of 85-41b was calculated using phase proportions and Fe-Mg exchange KD's based on the 200 MPa experiments on 85-41b reported in Grove et al. (2003). This calculation was necessary in order to carry out trace element modeling in Table 6

[d]Step 2, 0.14 opx + 0.16 cpx + 0.60 plag + 0.10 sp, $F = 0.8$ to 0.58

[e]PMA, 85-41c#9, 940°C, $F = 0.40$

[f]BA, 85-44# 5, 990°C, $F = 0.40$

the BA is An_{82} and the first plagioclase to crystallize in the PMA composition is An_{72}. As H_2O-saturated pressure drops the plagioclase Ca-Na K_D decreases and the first plagioclase to appear in the crystallization sequence becomes less An-rich. Therefore, the interpretation of the single peak in the Shastina lavas most consistent with the experimental data is that the Shastina lavas contain a mafic component similar to the PMA composition that crystallized at ~200 MPa, H_2O—saturated. The other eruptive phases of the stratocone appear to have received contributions from both an H_2O-rich BA parent as well as an H_2O-rich PMA parent.

Mafic inputs—summary

The combined evidence from all the phenocryst mineral compositions (Fo_{90} olivine, Mg# 90 augite, Mg# 82 orthopyroxene and An_{70} plagioclase) allow us to identify the dominant mafic component of the mixture as PMA. The PMA crystallizes this mineral assemblage at 200 MPa, H_2O-saturated at NNO. (Note that the presence of a slightly more magnesian orthopyroxene in some lavas implies crystallization at 100 MPa, H_2O-saturated or at higher fO_2). Thus, a pre-eruptive H_2O content of ~6 wt.% H_2O is indicated. The minimum pressure of this crystallization would be > 7 to ~9 km depth, or deeper if the melt was undersaturated or saturated with a mixed volatile fluid. However, the presence of Mg-rich amphibole and high H_2O contents in melt inclusions (10.8 wt.%) indicates the presence of an additional mafic component that experienced higher pressure fractional crystallization at pressures up to 900 MPa. In addition, the presence of high-An plagioclase (> An_{80}) implies the involvement of another mafic input with the composition of the BA, again at 200 MPa H_2O-saturated conditions.

Evolved end members of magma mixing

The identity of the evolved component(s) of the mixed Shasta lavas can not be inferred from the experiments carried out on the primitive Shasta region lavas by Grove et al. (2003). The most evolved component in the lavas appears to be a magma that was saturated with amphibole (Mg# 65–57), orthopyroxene (Mg# 55–60), plagioclase (An_{30-40}) and ilmenite/magnetite ± apatite. This mineral assemblage indicates the presence of a liquid that is more evolved than found in the lowest temperature experiments on the BA and PMA compositions (which have SiO_2 contents of ~59 and ~66 wt.%, respectively, on an anhydrous basis; Grove et al. 2003). The McKenzie Butte satellite vent to the south of Mt. Shasta (Fig. 2) is a rhyodacite (75-22, 85-42, 85-43, Table 1) that contains phenocrysts similar in composition to the most evolved mineral assemblage found in the frequency distribution of phenocryst cores from the stratocone andesite and dacite lavas, and it is assumed to represent one of the evolved end members of mixing. The intermediate peak that is present in the orthopyroxene (Mg# 65-70) and plagioclase (An_{40-50}) compositional histograms (Figs. 7, 8, 9, 10) indicates a third component similar to lowest temperature liquid and crystal assemblage produced in the PMA composition (Table 5, 85-41c #9) and this is assumed to represent the third component of the mixture. The evidence from the phenocryst populations represented in the Shasta andesite and dacite lavas indicates the presence of several magma reservoirs at different stages of evolution beneath the volcano. If this is the situation beneath the Mt. Shasta edifice when it is in an active phase, and it appears that it has been the case for all four of the eruptive stages, then there must be a set of physical conditions that has led to this hierarchy of magmas

chambers and a physical process that blends the lavas during stratocone eruptive events.

Trace element and isotopic variability between flows

A model for the origin of the trace element and isotopic variations observed in the primitive Mt. Shasta lavas is discussed in Grove et al. (2002). In their model the trace element compositional characteristics (Fig. 13a) have originated from melting of mantle peridotite and the addition of a subduction-related fluid-rich component. Grove et al. (2002) estimated the trace element budget of the fluid-rich component and suggested that it has been quite variable during the last ~200,000 years. The variability is attributed to contributions from different slab-derived components. One component has $^{87}Sr/^{86}Sr = 0.7028$ and $\varepsilon_{Nd} = +8$, and is most similar to a MORB source. The second component has more radiogenic $^{87}Sr/^{86}Sr = 0.7038$ and $\varepsilon_{Nd} = +1$ (Fig. 5) and is most similar to a sediment. These fluid-rich components probably represent a mixture of fluids and melts from the subducted lithosphere (serpentinized mantle, altered basalt, and sediment). Some elements (e.g., Sr and Ba, Figs. 4a, c and 13) are highly variable in abundance, and the wide range of variations in elemental abundances is ascribed to heterogeneity in the fluid-rich component.

Examination of each eruptive phase of the stratocone also reveals systematic variations in trace elements. Several of the Hotlum and Shastina lava flows were sampled along their entire length. These flows include the Shastina andesite flow that descends to the southwest of Shastina and is informally referred to as the Cascade Gulch flow (samples 96-1, 96-7, 96-5, 96-10) and two Hotlum flows, one informally referred to as the Military Pass flow to the northeast of Shasta (samples 82-91, 99-19) and the second informally referred to as the Ash Creek flow to the west of the Shasta summit (samples 99-14, 83-44). The systematics of major and trace element abundance variation were examined vs. distance from their respective vents and no compositional zoning was observed. The trace element abundances are essentially constant within each flow and diagnostic of that flow. A plot of Sr abundance vs. distance from the vent is shown for Hotlum and Shastina lavas in Fig. 13b. The variability in trace element abundances between separate flows is not accompanied by similarly large variations in major element abundances. In the case of the Shastina lavas this variation in trace element contents is extreme. The most primitive Shastina andesite flow (~5% MgO, 97-3, 99-4) has five times the Ba, two times the Sr and three times the Ce abundances of the other Shastina flows. Hotlum lava flows with essentially the same major element composition show between-flow Rb abundance differences of a factor of 1.5. These highly variable between-flow trace element abundances may be a reflection of heterogeneities inherited from the slab-derived fluid-rich component that initiates melting in the mantle wedge. Perhaps each flow represents a sample of a different fluid-induced flux-melting event in the mantle wedge.

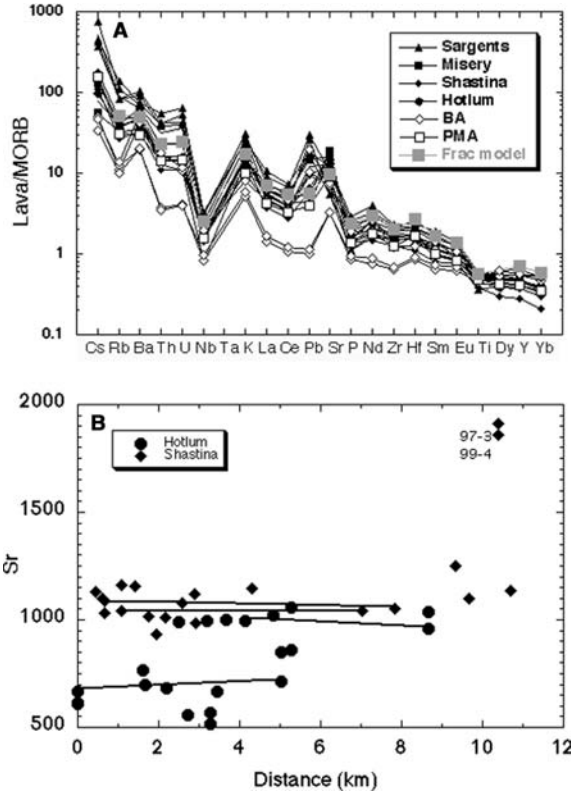

Fig. 13 **A** MORB-normalized multi-element diagram for Mt. Shasta region andesites and dacites and for the PMA and BA. Also shown are the calculated element abundances from the fractional crystallization model (Tables 5, 6) that produces a dacite liquid by fractional crystallization of a PMA starting composition. Normalizing values are from Sun and McDonough (1989). **B** Sr abundance in Shastina and Hotlum lavas plotted as a function of distance from their respective source vents. Samples from individual flows are connected by lines

Since most of the Shasta stratocone andesites are crystal-rich and the dominant phenocryst phase is plagioclase, one might ask whether variations in some of the trace element abundances are a consequence of crystal accumulation. Crystal accumulation effects have been examined by Baker (1988) who demonstrated that they were not important. Furthermore, some of the glassy Shastina lavas with $< 5\%$ phenocrysts of dominantly orthopyroxene and augite have the highest Sr abundance of all Shasta lavas (~1,900 ppm, 97-3 and 99-4, Fig. 4).

Crustal assimilation

An examination of the U-Th-Ra systematics in the Mt. Shasta stratocone andesite and dacite lavas led Newman et al. (1986) to conclude that crustal assimilation had occurred. Figures 4 and 13a show the results of a trace element model calculated for 58% fractional crystalli-

zation of a PMA parent magma to a dacite composition (Table 6). In general, the calculated element abundances fall within the range of trace element variations observed in the stratocone andesite, but there are some notable exceptions. Elements that would be concentrated in a crustal assimilant (Fig. 4, Rb, Ce and Zr, e.g., Grove et al. 1988) are higher in abundance in the evolved andesites than would be expected if fractional crystallization was the only magmatic process. Therefore, crustal assimilation is permitted by the data. However, the major element characteristics of the evolved andesites and dacites do not seem consistent with assimilation of average continental crust, which would contain much higher FeO*/MgO at high SiO_2 (Fig. 1b, which shows field encompassed by average andesitic crust). An alternative explanation for the high abundances of these trace elements may be by mixing small amounts of highly differentiated products of fractional crystallization that are present in the Shasta magmatic system. The production of such highly evolved residual liquids is an expected consequence of a long-lived magmatic system undergoing fractional crystallization, magma recharge and mixing.

Assimilation of ultramafic crust: the Trinity peridotite

The Trinity ultramafic complex is inferred to be present beneath Mt. Shasta (Fuis et al. 1987) and rare xenoliths of this material are present in the stratocone lavas. Thus, it is a potential source of high -Ni, -Cr and H_2O-rich (serpentinite) material for assimilation. Examination of the abundances of Ni and Cr (Fig. 4f, g) indicate that Mt. Shasta lavas define trends that are consistent with an origin by fractional crystallization from the high -Ni and -Cr primitive BA and PMA lavas. While it is not possible to completely rule out some assimilation, we note that the Ni-MgO and Cr-MgO trends completely overlap with the trends defined by the average global lava suites compiled by Ewart (1979, 1982) consistent with little or no assimilation. The mixed nature of the Shasta andesite and dacite lavas and the presence of xenocrystic olivine and spinel renders quantitative modeling of Ni and Cr variations difficult. However, one might hypothesize that the PMA and BA lavas are products of basalt—peridotite/serpentinite assimilation. This process can be ruled out on several grounds (see Baker et al. 1994). The Sr isotopic composition of the peridotite ($^{87}Sr/^{86}Sr = 0.7026$; Jacobsen et al. 1984) is uniformly depleted while the mafic BA and PMA inputs are highly variable (Fig. 5). The abundance of large ion lithophile, light rare earth and incompatible trace elements are directly correlated with H_2O content (Grove et al. 2002) and are hundreds to thousands of times higher in the primitive BA and PMA lavas than could ever be produced by assimilation of a mantle peridotite or serpentinite.

PMA as the dominant input into the Mt. Shasta magmatic system

The isotopic variations of the Mt. Shasta stratocone lavas show patterns of variations that are similar to those observed in all of the primitive BA and PMA lavas from the Shasta region (Fig. 5). However, the major element and mineral compositional evidence presented above indicates that the dominant parent magma for the Mt. Shasta stratocone andesites is the PMA with only minor contributions from BA input magma. A multi-

Table 6 Crystallization and magma mixing models that derive Shasta andesitic lavas

Fractionation model—trace elements

	Rb	Ba	Th	U	Nb	La	Ce	Pb	Sr	Nd	Zr	Hf	Sm	Eu	Y	Yb
Bulk partition coefficients used for modelling[a]																
Step 1	0.01	0.01	0.01	0.01	0.01	0.085	0.027	0.01	0.04	0.045	0.109	0.19	0.056	0.056	0.117	0.056
Step 2	0.016	0.13	0.018	0.04	0.18	0.127	0.05	0.65	1.42	0.047	0.052	0.08	0.046	0.065	0.048	0.065
Trace element abundances in fractionated melt of 85-41																
Step 1	17	189	1.69	0.68	3.6	10.7	24.2	1.2	812	12.9	92	3.45	2.6	0.85	12	1.05
Step 2	29	312	2.89	1.15	5.8	17.4	40.8	1.68	879	21.7	152	5.56	4.4	1.4	19.9	1.75

	SiO_2	TiO_2	Al_2O_3	FeO	MgO	CaO	Na_2O	K_2O	P_2O_5	R^2
Magma mixing models to produce average Shasta andesite major elements										
Andesite[b]	62.1	0.63	17.01	4.4	3.79	6.37	4.14	1.25	0.21	
Model 1	62.1	0.6	17	4.73	3.77	6.2	3.98	1.27	0.17	0.17
Model 2	62	0.56	17.4	4.88	3.8	5.78	4.1	1.25	0.14	0.83

Model 1[c]: 0.19 * 85-41b + 0.58 * 85-41c# 9 + 0.23 * 75-22
Model 2: 0.19 * 85-44 + 0.37 * 85-44# 5 + 0.44 * 75-22

[a]Trace element and rare earth element abundances calculated using the 85-41b fractional crystallization model in Table 5. Partition coefficient sources are similar to those in Grove et al. (1997)
[b]This is an average of all Shasta andesites reported in Table 1 with SiO_2 contents < 64 wt. %
[c]Least squares major element mixing model assumes a FARM (fractionation, assimilation, recharge and mixing) process similar to that discussed by Baker et al. (1991). See Table 5 for mixing components

component mixing model (Tables 5, 6) confirms that suggestion. The model uses two three-component mixtures: PMA + fractionated PMA dacite + McKenzie Butte rhyodacite and BA + fractionated BA + McKenzie Butte rhyodacite. The first combination produces the better match to an average of all Mt. Shasta andesites (both major- and trace-elements), and quantifies the conclusion drawn from qualitative examination of the major element systematics.

The conclusion that PMA is the dominant parent melt for the Shasta stratocone lavas leads to an interesting consequence. There is only one PMA eruptive center in the Mt. Shasta region and the lavas of this eruption have unique trace element, rare earth and isotopic characteristics (Figs. 4, 5, 13). The BA lavas show a range of isotopic and trace element variation that is much broader, encompasses that of the PMA and is more similar to (but not as extreme as) the range of variability in the stratocone andesite and dacite lavas. The logical inference is that the parental mantle—derived melts of the Mt. Shasta stratocone lavas are dominantly PMA—like in their major element characteristics but the trace element and isotopic characteristics of the PMA have been highly variable through time with variations similar to and more extreme than those found in the more abundant BA lavas from the Shasta region.

Model of the Mt. Shasta magmatic system

Figure 14 shows a schematic model of the magmatic processes consistent with the lava and mineral chemical variations that may have produced the Mt. Shasta stratocone andesite and dacite lavas. This view of multiple magma reservoirs in a complex plumbing system has been suggested for other volcanic centers as well; in Alaska (Power et al. 2002), New Zealand (Gamble et al. 1999; Nakagawa et al. 1999), the Lesser Antilles (Murphy et al. 2000; Pichavant et al. 2002), in Mexico (Cervantes and Wallace 2003) and elsewhere in the California Cascades (Donnelly-Nolan 1988).

In the case of Mt. Shasta, primitive H_2O-rich mantle melts are supplied to the crustal level magmatic system. These magmas have major element compositions similar to the PMA; high H_2O contents (4.5–6 wt.% or greater) and highly variable trace element abundances inherited from a subduction-derived fluid-rich component. In the Sargents, Misery and Hotlum cone-building stages, a minor amount of primitive BA magma also entered the magmatic system (required to account for the high-An plagioclase, Figs. 7, 8). These parental magmas rise into the shallow crust, fill and pond in magma reservoirs at ~7–10 km depth and undergo fractional crystallization to form evolved andesites/dacites (oliv + pyx fractionation in Fig. 14). This crystallization event leads to evolved melts that will crystallize magnesian orthopyroxene and augite and An_{55-70} plagioclase. When a BA magma undergoes

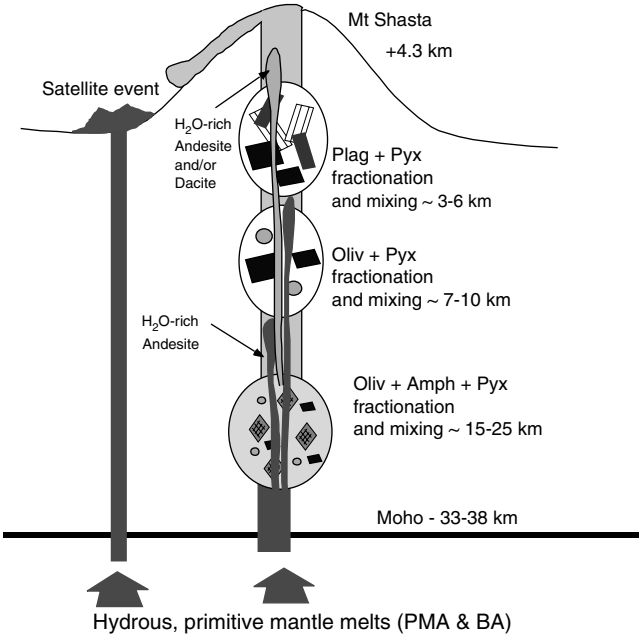

Fig. 14 Schematic representation of the crustal level fractional crystallization, magma recharge and magma mixing processes responsible for the generation of Mt. Shasta region andesites and dacites. A multitude of magmatic reservoirs are envisioned to be present beneath Mt. Shasta where fractional crystallization under high H_2O contents has generated andesite and dacite derivative liquids. Periodic recharge of these magma reservoirs by primitive parent magmas has produced multi-component mixed andesite and dacite lavas. The parent magma for most of the Mt. Shasta stratocone lavas is thought to be similar to the PMA in major elements and variable in trace element and isotopic compositions over a range spanned by all primitive Mt. Shasta region lavas

crystallization at this depth it produces magnesian augite and An-rich plagioclase ($>An_{80}$). The buoyant H_2O-saturated residual liquids produced by this fractional crystallization process, rise into shallower magma reservoirs (plag + pyx fractionation in Fig. 14). Cooling and crystallization continues and these evolved liquids fractionate to rhyodacite leaving crystalline products of Fe-rich amphibole and orthopyroxene (Mg# 65 and 55-65, respectively) and An_{30-40} plagioclase. During this time of crustal residence and fractional crystallization, the heat from crystallization may lead to limited crustal melting and assimilation. In addition, mineral compositional evidence suggests the operation of fractional crystallization of primitive magmas over a greater range of depths that extends as deep as the base of the crust (oliv + amph + pyx fractionation in Fig. 14). These deep products of fractional crystallization are also added to the magmatic system. The lavas produced during a stratocone summit eruption sample over a broad range of pressure/depth to produce multi-component mixed magmas.

A plot of the calculated density of Mt. Shasta region primitive lavas and stratocone andesites and dacites against MgO content is shown in Fig. 15. Lava compositions have been used to calculate liquid density

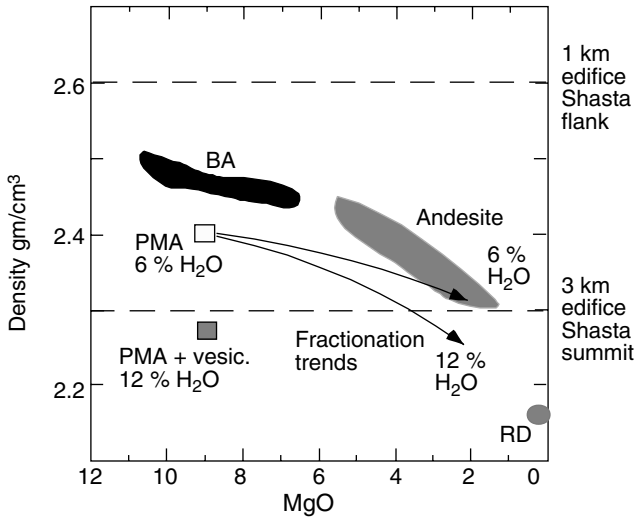

Fig. 15 Density vs. MgO plot for Mt. Shasta lavas. Labeled fields outline the density variations followed by Mt. Shasta BA, andesite, PMA and rhyodacite (RD) bulk compositions when calculated as liquids containing 6 wt.% H_2O. *Two arrows* from PMA show the effect of fractional crystallizations at constant H_2O (6 wt.%) and by allowing H_2O to increase to 12 wt.% (deep fractional crystallization model discussed in the text). *Horizontal dashed lines* show the critical magma density threshold for 1 and 3 km edifice heights taken from Pinel and Jaupart (2000). PMA + vesic represents the density change caused by vesiculation of a PMA magma that contains 12 wt.% H_2O

using the molar volume data of Bottinga and Weill (1970) modified by the addition of 6 wt.% H_2O (Ochs and Lange 1999). Also shown on the plot are the calculated densities of a primitive PMA liquid containing 6 wt.% H_2O, and fractionated dacite containing 6 wt.% H_2O and 12 wt.% H_2O as well as the critical melt densities for volcano edifice heights of 1 and 3 km from Pinel and Jaupart (2000, 2003). Critical melt densities are the predicted lower melt density limits above which magma can not rise through the volcanic overburden created by the edifice. For Mt. Shasta, an edifice height of 3 km is an appropriate model value. Primitive BA and PMA lavas are not expected to erupt from the summit, but have densities that are low enough to allow eruptions from flank vents (~1 km). Based on the edifice loading model the height of Mt. Shasta cone (~3 km) summit eruptions of andesite and dacite are permitted by the model if the H_2O contents are ~6 wt.%.

The processes that allowed repeated eruption of mixed magmas from the summit vents on Mt. Shasta clearly involved magma mixing followed by eruption, but what processes triggered mixing? If PMA magma is emplaced into a shallow crustal reservoir at 6 km depth at H_2O-saturated conditions, it will be denser than the overlying andesite and will remain trapped beneath the less dense, compositionally evolved andesites. However, if the primitive melts have a range of primary H_2O contents higher than 6 wt.%, or if fractional crystallization occurs at greater depth concentrating H_2O in the melt, and the differentiated products of this fractionation process ascend into the base of the magmatic plumbing system, a very buoyant melt will be supplied (e.g., $\rho = 2.27$ g cm^{-3} for a crystal-free andesite liquid containing 12 wt.% H_2O). This input of magma will be less dense than any of the differentiated melts in the magmatic system, and can mix with overlying primitive PMA, evolved dacite and rhyodacite. Thus, mixing caused by influx of deep, H_2O-rich melt may be a factor in triggering eruption. Evidence in support of a relation between mixing and eruption is the preservation of magnesian amphibole phenocrysts that surround olivine, orthopyroxene and augite. Breakdown rims on these high Mg# amphibole crystals are thin (~10 *mu*m), and indicate residence times of only days between mixing and eruption (Rutherford and Hill 1993). The lack of oxide re-equilibration also points to a time interval of days between mixing and eruption (Venezky and Rutherford 1997). The melt H_2O contents needed to stabilize the high Mg# amphibole could be as high as 15 wt.% H_2O and high H_2O contents found in Shastina melt inclusions (~11 wt.% H_2O, Grove et al. 2003) also point to high water contents in some Shasta magmas. Perhaps the influx of these magmas is part of the process that triggers the mixing and eruption through Mt. Shasta's edifice.

Buildup of magmatic gases in the sub-volcanic system could also lead to eruption (Jaupart and Allegre 1991), and could have been an important factor at Mt. Shasta. Therefore, another potential mechanism for decreasing the density of an ascending, underlying denser H_2O-rich mafic magma is by vesiculation (Eichelberger 1980). The pre-eruption state of the sub-volcanic crustal magmatic system beneath Mt. Shasta (Fig. 14) is one in which a series of magmas have stalled, cooled, degassed and crystallized. If a PMA liquid containing 10–15 wt.% H_2O ascends into a shallow magma reservoir at 200 MPa, it will exsolve 4–9 wt.% H_2O as bubbles. The density of these bubbles ($\rho = 0.3$–0.4 g cm^{-3}) will lower the density of the magma to 2.2–2.3 g cm^{-3}, so that the bulk primitive magma could also ascend through the overlying differentiated liquids present at shallower levels. Thus, vesiculation of high H_2O content magmas could also provide a mechanism for triggering mixing and eruption.

Conclusions

This paper has used the results of experiments performed on primitive magmas from the Mt. Shasta region and evidence preserved in Mt. Shasta stratocone lavas to develop a model for their origin. The major conclusions of this model are:

1. Primitive magnesian andesite (PMA, e.g., 85-41b, c, Baker et al. 1994) is the most suitable parent melt composition for the andesite and dacite lavas, but phenocryst evidence indicates that some primitive basaltic andesite (BA, e.g., 85-44 or 82-94a, Baker et al. 1994) was also introduced into the system.

2. The trace element and isotopic characteristics of the Mt. Shasta stratocone lavas indicate significant variations in the PMA parent magma. This compositional variability reflects variations in the input supplied from the subducted slab.
3. Magma mixing has been a persistent process in the development of the stratocone andesite and dacite lavas, and similar mixing processes involving similar end member components have operated to form stratocone lavas during each of Mt.Shasta cone building eruptive phases.
4. The Mt. Shasta magmatic system is characterized by very high H_2O contents: 6.5 wt.%. for the PMA parent and possibly up to 10 to 15 wt.% pre-eruptive H_2O contents for some input magmas. These high H_2O contents may be a factor in promoting the eruption of the multi-component mixed magmas. Fractional crystallization at deep crustal levels produces buoyant, high H_2O content magmas that can ascend into the magmatic plumbing system beneath Shasta, triggering mixing and eruption of the overlying primitive and evolved magmas.
5. Approximately 500 km^3 of andesite and dacite lavas have been erupted from Mt. Shasta in the last ~200,000 years; it is the largest volcano in the Cascade range. If one accepts that the PMA is the parent for the andesites, then this composition is a very abundant magma type in the total magmatic system. The volume of PMA input from the mantle is approximately 2.5 times the erupted mass represented in Mt. Shasta lavas or ~1,250 km^3.
6. Finally, the evidence discussed here underscores the problems of identifying the magmatic lineage of a subduction zone stratovolcano. There are varied inputs into the magmatic system beneath the Mt. Shasta stratocone. The existence of primitive melts at satellite vents and the rich diversity of mineralogical and trace element evidence preserved in the stratocone lavas allow these diverse inputs to be identified at this volcano.

Acknowledgements The authors thank J. Donnelly-Nolan, T. Sisson and P. Wallace for thoughtful reviews. The authors also thank R.L. Christiansen for sharing unpublished mapping and analyses of Mt. Shasta and for guidance in the collection of lavas discussed in this paper. This research was supported by National Science Foundation Grants EAR-9706214, EAR-0073766 and OCE-00001821.

References

Albee AL, Ray L (1970) Correction factors for electron probe microanalysis of silicates, oxides, carbonates, phosphates and sulfates. Anal Chem 42:1408–1414

Andersen DJ, Lindsley DH (1988) Internally consistent solution model for Fe-Mg-Mn oxides: Fe-Ti oxides. Am Mineral 73:714–726

Anderson AT (1974a) Evidence for a picritic, volatile-rich magma beneath Mt. Shasta, California. J Petrol 15:243–267

Anderson AT (1974b) Chlorine, sulfur and water in magmas and oceans. Geol Soc Am Bull 85:1585–1492

Anderson AT (1976) Magma mixing: petrological process and volcanological tool. J Volcan Geotherm Res 1:3–33

Anderson AT (1979) Water in some hypersthenic magmas. Jour Geol 87:509–531

Armstrong JT (1995) CITZAF—A package of correction programs for the quantitative electron microbeam x-ray analysis of thick polished materials, thin-films and particles. Microbeam Anal 4:177–200

Bacon CR, Druitt TH (1988) Compositional evolution of the zoned calcalkaline magma chamber at Mount Mazama, Crater Lake, Oregon. Contrib Mineral Petrol 98:224–256

Bacon CR, Bruggman PE, Christiansen RL, Clynne MA, Donnelly-Nolan JM, Hildreth W (1997) Primitive magmas at five Cascade volcanic fields: Melts from hot, heterogeneous sub-arc mantle. Can Mineral 35:397–423

Baker MB (1988) Evolution of lavas at Mt. Shasta volcano, N. California: an experimental and petrologic study. PhD Thesis, M.I.T.

Baker MB, Grove TL, Kinzler RJ, Donnelly-Nolan JM, Wandless GA (1991) Origin of compositional zonation (high-alumina basalt to basaltic andesite) in the Giant Crater lava field: Medicine Lake Volcano, northern California. J Geophys Res 96:21819–21842

Baker MB, Grove TL, Price R (1994) Primitive basalts and andesites from the Mt. Shasta region, N. California: products of varying melt fraction and water content. Contrib Mineral Petrol 118:111–129

Bence AE, Albee AL (1968) Empirical correction factors for the electron microanalysis of silicates and oxides. J Geol 76:382–403

Benz HM, Zandt G, Oppenheimer DH (1992) Lithospheric structure of northern California from teleseismic images of the upper mantle. J Geophys Res 97:4791–4807

Blakely RJ, Jachens RC, Simpson RW, Couch RW (1985) Tectonic setting of the southern Cascade Range as interpreted from its magnetic and gravity fields. Geol Soc Am Bull 96:43–48

Blakely RJ, Christiansen RL, Guffanti M, Wells RE, Donnelly-Nolan JM, Muffler MJP, Clynne MA, Smith JG (1997) Gravity anomolies, quaternary vents and quaternary faults in the southern Cascade range, Oregon and California: Implications for backarc evolution. J Geophys Res 102:22513–22507

Blatter DL, Carmichael ISE (1998) Plagioclase-free andesites from Zitacuaro (Michoacan), Mexico: petrology and experimental constraints. Contrib Mineral Petrol 132:121–138

Bottinga Y and Weill D (1970) Densities of liquid silicate systems calculated from partial molar volumes of oxide components. Am J Sci 269:169–182

Cervantes P, Wallace PJ (2003) Magma degassing and basaltic eruption styles: a case study of ~2000 ybp Xitle volcano in central Mexico. J Volcanol Geotherm Res 120:249–270

Christiansen RL, Kleinhampl FJ, Blakely RJ, Tuchek ET, Johnson FL, Conyac MD (1977) Resource appraisal of the Mt. Shasta wilderness study area, Siskiyou County, California. Open-file Report 77–250, U.S. Geol. Survey, p 53

Condie KC, Swenson DH (1973) Compositional variation in three Cascade stratovolcanoes: Jefferson, Rainer, Shasta. Bull Volcanol 37:205–230

Donnelly-Nolan JM (1988) A magmatic model of Medicine Lake volcano, California. J Geophys Res 93:4412–4420

Eichelberger JC (1980) Vesiculation of mafic magma during replenishment of silicic magma reservoirs. Nature 288:446–450

Ewart A (1979) A review of the mineralogy and chemistry of Tertiary-Recent, dacitic, latitic, rhyolitic and related sialic rocks. In: Barker F (ed) Trondjhemites, dacites and related rocks. Elsevier, Amsterdam, pp 13–121

Ewart A (1982) The mineralogy and petrology of Tertiary-Recent orogenic volcanic rocks: with special reference to the andesite-basaltic compositional range. In: Thorpe RS (ed) Andesites. Wiley, New York, pp 25–95

Fuis GS, Zucca JJ, Mooney WD, Milkereit B (1987) A geologic interpretation of seismic-reflection results in northern California. Geol Soc Am Bull 98:53–65

Gaetani GA, Grove TL (1998) The influence of water on melting of mantle peridotite. Contrib Mineral Petrol 131:323–346
Gamble JA, Wood P, Price RC, Smith IEM, Waight TE, (1999) A fifty year perspective of magmatic evolution on Ruapehu Volcano, New Zealand: Verification of open system behaviour in an arc volcano. Earth Planet Sci Lett 170:301–314
Gill JB (1981) Orogenic andesites and plate tectonics. Springer, Berlin Heidelberg New York, p 390
Griscom A (1980) Klamath Mountains province. In: Oliver H (ed) Interpretation of the Gravity Map of California and its Continental Margin, Calif Div Mines Bull 205:34–36
Grove TL, Juster TC (1989) Experimental investigations of low-Ca pyroxene stability and olivine–pyroxene–liquid equilibria at 1-atm in natural basaltic and andesitic liquids. Contrib Mineral Petrol 103:287–305
Grove TL, Kinzler RJ, Baker MB, Donnelly-Nolan JM, Lesher CE (1988) Assimilation of granite by basaltic magma at Burnt lava flow, Medicine Lake volcano, northern California: decoupling of heat and mass transfer. Contrib Mineral Petrol 99:320–343
Grove TL, Donnelly-Nolan, Housh T (1997) Magmatic processes that generated the rhyolite of Glass Mountain, Medicine Lake volcano, N. California. Contrib Mineral Petrol 127:205–223
Grove TL, Parman SW, Bowring SA, Price RC, Baker MB (2002) The role of an H_2O-rich fluid component in the generation of primitive basaltic andesites and andesites from the Mt. Shasta region, N. California. Contrib Mineral Petrol 142:375–396
Grove TL, Elkins-Tanton LT, Parman SW, Müntener O, Gaetani GA (2003) Fractional crystallization and mantle melting controls on calc-alkaline differentiation trends. Contrib Mineral Petrol 145:515–533
Harris SL (2003) Fire Mountains of the West: The Cascades and Mono Lake volcanoes. Mountain Press, p 372
Huebner JS, Sato M (1970) The oxygen fugacity-temperature relationships of manganese and nickel oxide buffers. Am Mineral 55:934–952
Irvine TN, Baragar WRA (1971) A guide to the chemical classification of the common volcanic rocks. Can J Earth Sci 8:523–548
Jacobsen SB, Quick JE, Wasserburg GJ (1984) A Nd and Sr isotopic study of the Trinity peridotite; implications for mantle evolution. Earth Planet Sci Lett 68:361–378
Jaupart C and Allegre CJ (1991) Gas content, eruption rate and instabilities of eruption regime in silicic volcanoes. Earth Planet Sci Lett 102:413–429
Kay RW (1978) Aleutian magnesian andesites: melts from subducted Pacific oceanic crust. J Volcanol Geotherm Res 4:117–132
MacDonald GA (1966) Geology of the Cascade Range and Modoc Plateau. In: Bailey EH (ed) Geology of Northern California. Calif Div Mines Bull vol 190, pp 65–95
Miller CD (1978) Holocene pyroclastic deposits from Shastina and Balck Butte, west of Mount Shasta, California. J Res US Geol Surv 6:611–624
Miller CD (1980) Potential hazards from future eruptions in the vicinity of Mount Shasta volcano, northern California. Geol Surv Bull 1503:43
Moore G, Carmichael ISE (1998) The hydrous phase equilibria (to 3 kbar) of an andesite and basaltic andesite from western Mexico: Constraints on water content and conditions of phenocryst growth. Contrib Mineral Petrol 130:304–319
Murphy MD, Sparks RSJ, Barclay J, Carroll MR, Brewer TS (2000) Remobilization of andesite magma by intrusion of mafic magma at Soufriere Hills volcano, Montserrat, West Indies. J Petrol 41:21–42
Nakagawa M, Wada K, Thordarson T, Wood CP, Gamble JA (1999) Petrological investigations of the 1995 and 1996 eruptions of Ruapehu Volcano, New Zealand: formation of discrete and small magma pockets and their intermittent discharge. Bull Volcanol 61:15–31
Newman S, MacDougall JD, Finkel RC (1986) Petrogenesis and ^{230}Th–^{238}U disequilibrium at Mt. Shasta, California and in the Cascades. Contrib Mineral Petrol 93:195–206
Norrish K, Chappel BW (1977) X-ray fluorescence spectrography. In: Zussman J (ed) Physical methods in determinative mineralogy. Academic Press, New York, p 514
Norrish K, Hutton JT (1969) An accurate x-ray spectrographic method for the analysis of geologic samples. Geochim Cosmochim Acta 33:431–454
Ochs FA, Lange RA (1999) The density of hydrous magmatic liquids. Science 283:314–317
Pichavant M, Martel C, Bourdier J-L, Scaillet B (2002) Physical conditions, structure and dynamics of a zoned magma chamber: Mont Pelee (Martinique, Lesser Antilles Arc). J Geophys Res 107. DOI 10.1029/2001JB000315
Pinel V, Jaupart C (2000) The effect of edifice load on magma ascent beneath a volcano. Phil Trans R Soc London A 358:1515–1532
Pinel V, Jaupart C (2003) Magma chamber behavior beneath a volcanic edifice. J Geopys Res 108(B2):2072. DOI 10.1029/2002JB001751
Power JA, Jolly AD, Nye CJ, Harbin ML (2002) A conceptual model for the Mount Spur magmatic system from seismic and geochemical observations of the 1992 Crater peak eruption sequence. Bull Volcanol 64:206–218
Rutherford MJ and Hill PM (1993) Magma ascent rates from amphibole breakdown—an experimental study applied to the 1980–1986 Mount St. Helens eruptions. J Geophys Res 98:19667–19685
Sisson TW, Bacon CR (1999) Gas driven filter pressing in magmas. Geology 27:613–616
Sisson TW, Grove TL (1993) Temperature and H_2O contents of low-MgO high-alumina basalts. Contrib Mineral Petrol 113:167–184
Sisson TW, Layne (1993) H_2O in basalt and basaltic andesite glass inclusions from four subduction—related volcanoes. Earth Planet Sci Lett 117:619–635
Smith AL, Carmichael ISE (1968) Quaternary lavas from the southern Cascades, western USA. Contrib Mineral Petrol 19:212–238
Sun SS, McDonough WD (1989) Chemcial and isotopic systematics of oceanic basalts: implications for mantle composition and p rocesses. In: Saunders AD, Norry MJ (eds) Magmatism in Ocean Basins. Geol Soc Spec Publ 42:313–345
Symonds RB, Rose WI, Bluth GSJ, Gerlach TM (1994) Volcanic gas studies: methods, results and applications. In: Carroll MR, Holloway JR (eds) Reviews in Mineralogy, version 30, Volatiles in magmas, Mineralogical Society of America, p 517
Tatsumi Y, Ishizaka K (1982) Origin of high-magnesian andesites in the Setouchi volcanic belt, southwest Japan, I. Petrographical and chemical characteristics. Earth Planet Sci Lett 60:293–304
Venezky DY, Rutherford MJ (1997) Preeruption conditions and timing of dacite-andesite magma mixing in the 2.2 ka eruption at Mt. Rainer. J Geophys Res 102:20069–20086
Volpe AM (1992) $^{238}U-^{230}Th-^{226}Ra$ disequilibrium in young Mt. Shasta andesites and dacites. J Volcanol Geotherm Res 53:227–238
Williams H (1932a) Geology of the Lassen Volcanic National Park, California. Calif Univ Dept Geol Sci Bull 21:195–385
Williams H (1932b) Mount Shasta, a Cascade volcano. J Geol 45:417–429
Williams H (1934) Mount Shasta, California. Zeitschr Vulkan 15:225–253
Williams H (1949) Geology of Macdoel quadrangle (California). Calif Div Mines Bull 151:7–60
Yogoszinski GM, Kay RW, Volynets ON, Koloskov AV, Kay SM (1995) Magnesian andesite in the western Aleutian Komandorsky region: implications for slab melting and processes in the mantle wedge. Geol Soc Am Bull 107:505–519